Mechanics of Advanced Composite Structures 14 (2027), Serial Number 29, 75 – 97

Mechanics of Advanced Composite Structures

Journal homepage: https://macs.semnan.ac.ir/

Semnan University

ISSN: 2423-7043

Research Article

Dynamic Analysis of Functionally Graded Nanobeams Using Various Shear Deformation Theories Based on Doublet Mechanics

Alireza Javanbakht, Morteza Karamooz Mahdiabadi *

Department of Mechanical Engineering, Tarbiat Modares University, Tehran, 1464753111, Iran

ARTICLE INFO

Article history:

Received: 2025-03-19
Revised: 2025-11-28
Accepted: 2026-01-02

Keywords:

Functionally Graded materials;
Vibration analysis;
Doublet mechanics;
Rayleigh-Ritz method;
Nanostructure.

ABSTRACT

This study investigates the vibrational behavior of a functionally graded beam using the doublet mechanics theory. This theory accounts for interactions between constituent atoms within a structure, enabling consideration of atomic-scale structure and orientation relative to the beam axis. While classical Euler–Bernoulli and Timoshenko beam theories are commonly used within the framework of doublet mechanics, they typically neglect key terms associated with shear deformation effects. To overcome this limitation, the present research introduces the novel application of higher-order shear deformation theories (HSDTs) within the doublet mechanics framework. This approach, not previously explored in the literature, provides more accurate predictions of vibrational characteristics. The results reveal that employing doublet mechanics can significantly influence natural frequencies, with deviations of up to 5%.

1. Introduction

Functionally graded (FG) materials can be found in nature, such as dental crowns that consist of FG materials because they are hard and wear-resistant on the outside but ductile on the inside [1, 2]. The first proposal of FG materials for industrial applications was made in 1984-1985 during the development of a Japanese space plane project. The space plane's exposure to high temperatures and thermal gradients necessitated the use of materials that exhibit tailored thermal and structural properties. There were no substances with proper properties for that application, so FG materials were fabricated [2, 3]. FG materials have since been widely used in various industries due to their unique properties, including their ability to provide tailored mechanical and thermal properties, so various research has been done on functionally graded materials [4, 5].

The FG materials are mostly a combination of ceramic and metal. The ceramic component has low thermal conductivity, so it can resist high

* **Corresponding author.**
E-mail address: karamooz@modares.ac.ir

Cite this article as:

Javanbakht, A. and Karamooz Mahdiabadi, M., 2027. Dynamic Analysis of Functionally Graded Nanobeams Using Various Shear Deformation Theories Based on Doublet Mechanics. *Mechanics of Advanced Composite Structures*, 14(1), pp. 75-97.

https://doi.org/10.22075/MACS.2026.37204.1823

temperature, and the metal component can resist stress concentration [6].

Although there are some investigations about axially graded FG beams [7, 8], in most cases, FG beams in which material properties vary along the thickness have been investigated. Vibration of FG beams has been investigated in several papers. Jin and Wang [9] used the weak form quadrature element method to investigate the free vibration of FG beams. They investigated the effect of the power-law index on the first five eigenfrequencies of functionally graded beams with different boundary conditions. The results demonstrated that an increase in the power-law index leads to a decrease in eigenfrequencies because a higher power-law index means that the material is closer to metal, and ceramic behavior is vanishing, so eigenfrequencies decrease. Free vibration of a size-dependent FG microbeam has been investigated by (FSDBT) (strain gradient Timoshenko). Results showed that thickness has a significant effect on natural frequencies, which cannot be noticed when using CBT [10]. Attia [11] has investigated the static and dynamic response of an FG beam based on the nonlocal-couple-stress-surface elasticity (NLCSSE) model. Dehrouyeh-Semnani et al. [12] have investigated Free vibration of FG microbeams by using the modified couple stress theory. Modified couple stress theory was also used for vibration analysis of a three-dimensional rotating FG microbeam [13]. Rahmani et al. [14] have also used the modified couple stress theory to investigate the vibration of an FG microbeam that carries an attached mass. Some researchers [15, 16] have investigated FG beam natural frequencies using Euler-Bernoulli and Timoshenko beam theories. Pradhan and Chakraverty [6] did research on free vibration of FG beams by the Rayleigh-Ritz method using CBT and FSDBT. In some other research, higher-order shear deformation beam theories have been used to investigate free vibration of a composite beam [17-20].

As it was mentioned before, FG materials were fabricated because of their thermal qualities, so some works have focused on the temperature-dependent vibration of FG beams. Babaei et al. [21] investigated temperature-dependent vibration of FG microbeams by modified coupled stress theory. The model was based on CBT, and Galerkin's approximate method has been used.

Due to increasing usage of nano and microstructures and composites, the dynamics and vibration of such structures have been the subject of various research works [22-26]. Uzun and Yayli [27] investigated the deformable boundary effect on dynamic of FG nanobeams embedded in the Winkler-Pasternak medium. Also, high-frequency analysis of exponentially graded nanobeams resting on Winkler–Pasternak foundations has been investigated [28]. The FG sandwich doubly curved nano shells have been dynamically analyzed using variable nonlocal elasticity theory [29].

In micro and nano scale structures, mechanical properties and behavior may significantly differ from those seen in macro scale structures. Additionally, new parameters that do not affect the vibrational behavior of macro structures considerably may noticeably influence the vibration results of micro and nano beams. As a result, some traditional theories may not appropriately describe the behavior of micro and nano beams, and the effect of some parameters may be neglected or not considered in these theories. Among various nanoscale theories, the doublet mechanics theory stands out due to its multi-scale nature [30], offering advantages over other models. Additionally, while most size-dependent theories are limited to predicting either softening or hardening behavior, the doublet mechanics theory predicts both [31]. The atomic structure of a beam is a parameter that is not typically considered in common beam theories, yet it can have a significant impact on the dynamic behavior of micro and nano beams. By incorporating DM theory, this parameter can be taken into account. This advanced theory allows for the investigation of the effects of atomic structure, including the atomic bond length and angle of the atomic structure with respect to the beam's longitudinal direction.

The DM theory was first proposed by Granik [32]. Later, Granik and Ferrari [33] applied DM theory to granular materials and derived kinematic equations for granular materials using DM theory [30]. The atomic structure plays a critical role in the behavior of nanostructures. By incorporating DM theory, it is possible to improve the accuracy of the estimated vibrational behavior of these structures.

Gul et al. [34] investigated the axial vibration of a nanorod embedded in an elastic medium using DM theory. Noncoaxial vibration of embedded double-walled carbon nanotubes (CNT) using DM theory was also investigated [35]. Furthermore, the vibration analysis of an Euler-Bernoulli FG nanobeam with periodic nanostructure using DM theory was studied [31],

and a similar analysis of a Timoshenko nanobeam using DM theory was conducted [36]. Abdelrahman et al. [37, 38] studied the effect of moving load on the dynamics of nanoscale Timoshenko CNTs based on DM theory. Also, the vibration of imperfect and curved CNTs using DM has been studied [39, 40]. Civalec et al. [41] investigated the longitudinal vibration of FG nanorods using DM.

Some terms in the DM formulation are equal to zero while using classical Euler-Bernoulli and Timoshenko theories in nanobeams. In this research, the higher-order shear deformation theories have been used to bring those terms into consideration and enhance the precision of calculations, which has not been studied before. Furthermore, in this research, the vibrational behavior of an FG nanobeam with an in-plane atomic bond angle of 120 degrees using DM theory is investigated, which has not been previously done.

To sum up, this research aims to investigate the vibrational behavior of an FG nanobeam through the use of DM theory and higher-order shear deformation theories. We will also analyze the FG structure with an in-plane atomic bond angle of 120 for two different angles of atomic structure with respect to the beam's longitudinal direction. Additionally, we will compare the results obtained from DM theory with those obtained from the classical method and discuss the results.

2. Functionally Graded Material

FG materials are a special kind of composite material made up of a combination of metal and ceramic. The FG beam being investigated in this research features pure metal at the bottom surface and pure ceramic on the top surface. The mechanical characteristics of the beam change along its thickness, as described in Eq. 1 [31]:

$$P(z) = (P_c - P_m)\left(\frac{z}{h} + 0.5\right)^k + P_m \quad (1)$$

Among the exponential, power, and sigmoid laws commonly used to describe property variations in functionally graded (FG) beams, the power law index captures these variations most distinctly. Therefore, to explore a broader range of FG material configurations, the power law has been adopted in this study.

In the FG beam being investigated, the mechanical properties change along with its thickness. This change is justified by the power-law index. k, which is described in Eq. 1, where P_m represents the metal properties, and P_c represents the ceramic properties. This equation allows for the calculation of the elasticity modulus and density of the beam along its thickness, as described in Eq. 2 and Eq. 3, respectively [31]:

$$E(z) = (E_c - E_m)\left(\frac{z}{h} + 0.5\right)^k + E_m \quad (2)$$

$$\rho(z) = (\rho_c - \rho_m)\left(\frac{z}{h} + 0.5\right)^k + \rho_m \quad (3)$$

As it is self-explanatory, at the bottom surface where $z = -h/2$, properties are equal to those of metal, and on the top surface, where $z = +h/2$, properties are equal to ceramics', and along the thickness, properties are a combination of metal and ceramic. A schematic of the considered beam is shown in Fig. 1.

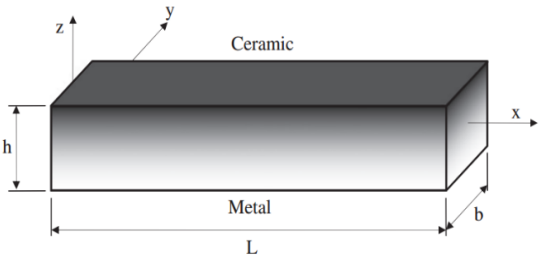

Fig. 1. Functionally Graded beam [17]

3. Formulation of Hamilton Method

To investigate the free vibration analysis of the nanobeam, we use the extended Hamilton's principle, which consists of the strain and kinetic energies (assuming no applied loads). The strain energy of the beam can be written as [42]:

$$U_s = \frac{1}{2}\iiint (\sigma_{xx}\varepsilon_{xx} + \tau_{xz}\gamma_{xz})dv \quad (4)$$

where

$$\sigma_{xx} = A_{xx}\varepsilon_{xx} \quad (5)$$

$$\tau_{xz} = \kappa A_{xz}\gamma_{xz} \quad (6)$$

where σ_{xx} is the normal stress, τ_{xz} is the shear stress, ε_{xx} is the normal strain and γ_{xz} is the shear strain.

A_{xx} and A_{xz} are the FG material constants computed by Eq. 1, relating the stress and strain [42]:

$$A_{xx} = (E_c - E_m)\left(\frac{z}{h} + 0.5\right)^k + E_m \quad (7)$$

$$A_{xz} = (\mu_c - \mu_m)\left(\frac{z}{h} + 0.5\right)^k + \mu_m \quad (8)$$

$$\mu_m = \frac{E_m}{2(1+\nu_m)} \quad (9)$$

$$\mu_c = \frac{E_c}{2(1+\nu_c)} \quad (10)$$

where ν_m and ν_c are poisson ratio of the metal and ceramic, respectively, and κ (kappa) is a coefficient that depends on the shear deformation theory that is being used, E is the modulus of elasticity and μ is shear modulus.

Normal deformation is calculated as [18]:

$$U_s = u - z\frac{\partial w}{\partial x} + f_z(\frac{\partial w}{\partial x} - \varphi) \quad (11)$$

where u is axial displacement, w is transversal displacement along z axis, ϕ is $\frac{\partial w_b}{\partial x}$ which is the angle of axial displacement caused by bending and f_z is determined by the shear deformation theory, which is being used. f_z and κ for different shear deformation theories are shown in Table 1. It should be noted that previous works have not studied the effect of higher-order shear deformation theories in DM theory. The shear deformation functions bring shear stress into consideration and enhance the precision of vibration and buckling calculations significantly; specially in FG beams and structures[43-45].

Table 1. f_z for different shear deformation theories

Theory	f_z	κ
CBT (Euler-Bernoulli)	0	1
FSDBT (Timoshenko)	z	$\frac{5}{6}$
PSDBT (Parabolic)	$z\left(1-\frac{4z^2}{3h^2}\right)$	1
TSDBT (Trigonometric)	$\frac{h}{\pi}\sin\left(\frac{\pi z}{h}\right)$	1
HSDBT (Hyperbolic)	$h\sinh\left(\frac{z}{h}\right) - z\cosh(0.5)$	1
ESDBT (Exponential)	$ze^{-2\left(\frac{z}{h}\right)^2)}$	1

The shear strain and normal strain are calculated in the following way [18]:

$$\varepsilon_{xx} = \frac{\partial U_s}{\partial x} = \frac{\partial u}{\partial x} - z\frac{\partial^2 w}{\partial x^2} + f_z\frac{\partial^2 w}{\partial x^2} - \frac{\partial \varphi}{\partial x} \quad (12)$$

$$\gamma_{xz} = 2\varepsilon_{xz} = \frac{\partial U_s}{\partial z} + \frac{\partial w}{\partial x} = -\frac{\partial w}{\partial x} + \left(\frac{\partial w}{\partial x} - \varphi\right)\frac{df_z}{dz} + \frac{\partial w}{\partial x}$$
$$= (\frac{\partial w}{\partial x} - \varphi)\frac{df_z}{dz} \quad (13)$$

By substituting Eq. 7, Eq. 8, Eq. 12 and Eq. 13 in Eq. 4, Eq. 5 and Eq. 6 and integrating over width, height and length of the beam, the strain energy is calculated. Due to the fact that there is no change in material properties through the width of the beam, the kinetic energy is computed as Eq. 14 [36]:

$$T = \frac{1}{2}b\int_0^L\int_{-0.5h}^{0.5h}((\rho_c - \rho_m)\left(\frac{z}{h} + 0.5\right)^k + \rho_m)(\frac{\partial U_x^2}{\partial t} + \frac{\partial U_z^2}{\partial t})dv \quad (14)$$

$$u_x = U_s \quad (15)$$

$$u_z = w \quad (16)$$

4. Formulation of the Doublet Mechanics Method

The DM theory considers two adjacent parts or atoms as a doublet and incorporates a length scale parameter to account for their distance from each other. This parameter is demonstrated in Fig. **2** by η_α and can correspond to the atomic bond length between two adjacent atoms.

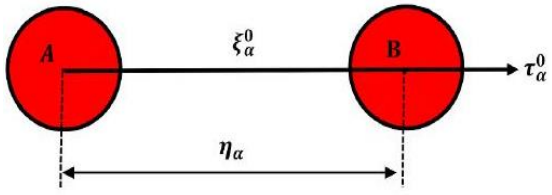

Fig. 2. A doublet in doublet mechanics theory [46]

The DM theory considers the interactions between atoms or parts to determine the mechanical behavior of the whole structure. This theory accounts for stretching, shearing, and torsional interactions between doublets. However, for the sake of simplicity and to reduce computational costs, this paper only considers stretching interactions. The stretching displacement of the doublet α is [46] :

$$\Delta u_\alpha = \xi_\alpha - \xi_\alpha^0 \quad (17)$$

where ξ_α^0 is the initial distance between nodes and ξ_α is the distance of nodes in the present time. Then, by DM assumptions Δu_α can be calculated by Eq. 18 in the Cartesian coordinate[46] :

$$\Delta u_\alpha = \sum_{\chi=1}^{M}\frac{\eta_\alpha^\chi}{\chi!}\tau_{\alpha k1}^0\tau_{\alpha k2}^0 \dots \tau_{\alpha k\chi}^0\frac{\partial^\chi u_i}{\partial x_{k1}\,\partial x_{k2}\dots\partial x_{k\chi}} \quad (18)$$

where $k1$, $k2$ ... $k\chi$ are equal to 1, 2, and 3 in cartesian coordinate and in this paper 1 is x, 2 is y, and 3 is z axes.

According to Fig. 2, τ_a is the unit vector along the direction of α th bond and τ_{ak1} is its picture in the direction of k1 axis. Therefore $\eta_\alpha \tau^0_{\alpha k1}$ is the projection of a^{th} bond in k1 direction, as it is illustrated in Fig. 2 and Fig. **3**. So, the stretching micro-strain is [46]:

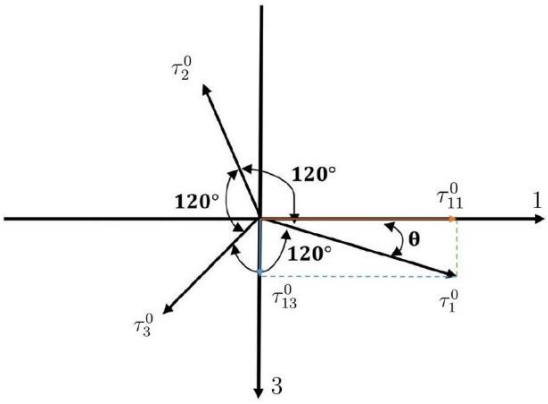

Fig. 3. Three doublets with equal angles with respect to each other

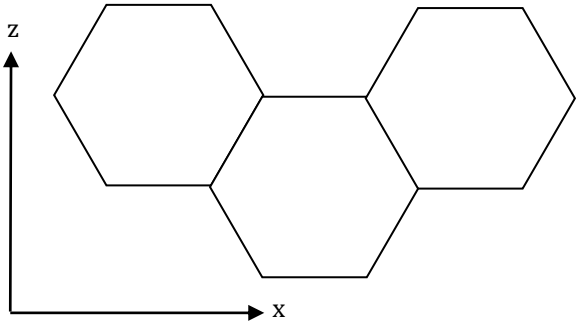

(a)

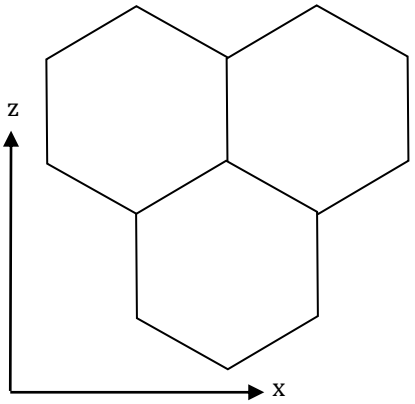

(b)

Fig. 4. Microstructure along beam length: a) Zigzag, b) Armchair

$$\varepsilon_a = \frac{\tau^0_{\alpha i} \Delta u_\alpha}{\eta_\alpha} = \tau^0_{\alpha i} \sum_{\chi=1}^{M} \frac{\eta_\alpha^{\chi-1}}{\chi!} \tau^0_{\alpha k1} \tau^0_{\alpha k2} \dots \tau^0_{\alpha k\chi} \frac{\partial^\chi u_i}{\partial x_{k1}\, \partial x_{k2} \dots \partial x_{k\chi}} \tag{19}$$

where $\chi!$ in factorial of χ. By setting values of 1 to 3, the components of ε_a in the direction of x, y and z are calculated.

The relation between microstress and micro strain is [46] :

$$p_a = \sum_b A_{ab}\, \varepsilon_b \tag{20}$$

where A_{ab} is a micro module of the elasticity of doublet. A_{ab} is defined as[46]:

$$A_{\alpha\beta} = \begin{bmatrix} \frac{4}{9}\mu\frac{7\lambda+10\mu}{\lambda+2\mu} & \frac{4}{9}\mu\frac{\lambda-2\mu}{\lambda+2\mu} & \frac{4}{9}\mu\frac{\lambda-2\mu}{\lambda+2\mu} \\ \frac{4}{9}\mu\frac{\lambda-2\mu}{\lambda+2\mu} & \frac{4}{9}\mu\frac{7\lambda+10\mu}{\lambda+2\mu} & \frac{4}{9}\mu\frac{\lambda-2\mu}{\lambda+2\mu} \\ \frac{4}{9}\mu\frac{\lambda-2\mu}{\lambda+2\mu} & \frac{4}{9}\mu\frac{\lambda-2\mu}{\lambda+2\mu} & \frac{4}{9}\mu\frac{7\lambda+10\mu}{\lambda+2\mu} \end{bmatrix} \tag{21}$$

$$\lambda = \frac{\nu E}{(1+\nu)(1-2\nu)} \tag{22}$$

$$\mu = \frac{E}{2(1+\nu)} \tag{23}$$

$$\nu = \frac{\lambda}{2(\lambda+\mu)} \tag{24}$$

The in-plane stress assumption is $\lambda = 2\mu$. By putting $\nu = \frac{1}{3}$ in Eq. 24, $A_{ii} = A_0$ is given by [46]:

$$A_0 = \frac{4}{9}\mu\frac{7\lambda+10\mu}{\lambda+2\mu} = \frac{8\mu}{3} = E \tag{25}$$

The stretching macro stress relation based on Ferrari [47]is achieved by:

$$\sigma_{ik1} = \tau^0_{ai} \sum_{a=1}^{m} \tau^0_{ak1} \sum_{\chi=1}^{M} (-1)^{\chi-1} \left(\frac{\eta_\alpha^{\chi-1}}{\chi!} \tau^0_{ak2} \dots \tau^0_{ak\chi} \frac{\partial^{\chi-1} p_{ai}}{\partial x_{k2} \dots \partial x_{k\chi}} \right) \tag{26}$$

The previous works have indicated that using 3 terms of the Taylor series in Eq. 26 can provide satisfactory results for DM theory [36, 46]. Therefore, using this assumption and keeping the terms that contain η_a upto the second power (for the sake of lowering the computational costs terms that contain η_a with a power more than 2 are neglected), Eq. 26 is written as [36]:

$$\sigma_{ij} = \sum_{\alpha=1}^{m} A_0\, \tau^0_{\alpha i} \tau^0_{\alpha j} \tau^0_{\alpha m} \tau^0_{\alpha n} \left(\varepsilon_{mn} + \frac{\eta_\alpha^2}{12} \tau^0_{\alpha t} \tau^0_{\alpha s} \frac{\partial^2 \varepsilon_{mn}}{\partial x_t\, \partial x_s} \right) \tag{27}$$

According to Fig. 3, τ_{ij} is calculated by Eq. 28 [46]:

$$\tau_{ij} = \begin{bmatrix} cos(\theta) & cos(90) & sin(\theta) \\ cos(\theta + 240) & cos(90) & sin(\theta + 240) \\ cos(\theta + 120) & cos(90) & sin(\theta + 120) \end{bmatrix} \quad (28)$$

here, θ represents the angle between the atomic structure and the beam's longitudinal axis. When θ=0, this arrangement is known as the "Zigzag structure". In this case, the atomic configuration along the beam length corresponds to that shown in Fig 4(a). Thus, for $\theta = 0$, τ_{ij} is [46]:

$$\tau_{ij} = \begin{bmatrix} 1 & 0 & 0 \\ -\frac{1}{2} & 0 & \frac{-\sqrt{3}}{2} \\ -\frac{1}{2} & 0 & \frac{\sqrt{3}}{2} \end{bmatrix} \quad (29)$$

Conversely, when $\theta = \frac{\pi}{6}$, the arrangement is referred to as the "Armchair structure" illustrated in fig. 4(b). For $\theta = \frac{\pi}{6}$, τ_{ij} is [46]:

$$\tau_{ij} = \begin{bmatrix} \frac{\sqrt{3}}{2} & 0 & \frac{1}{2} \\ 0 & 0 & -1 \\ \frac{-\sqrt{3}}{2} & 0 & \frac{1}{2} \end{bmatrix} \quad (30)$$

By substituting Eq. 29 into Eq. 27, the stress-strain relation for $\theta = 0$ will be[46]:

$$\sigma_{xx} = E\left(\varepsilon_{xx} + \frac{\eta_\alpha^2}{12}\frac{\partial^2 \varepsilon_{xx}}{\partial x^2} + \frac{\eta_\alpha^2}{32}\frac{\partial^2 \varepsilon_{xz}}{\partial x\, \partial z}\right) \quad (31)$$

$$\sigma_{xz} = E\left(\frac{3}{4}\varepsilon_{xx} + \frac{\eta_\alpha^2}{64}\frac{\partial^2 \varepsilon_{xz}}{\partial x^2} + \frac{3\eta_\alpha^2}{64}\frac{\partial^2 \varepsilon_{xz}}{\partial z^2}\right) \quad (32)$$

and for $\theta = \frac{\pi}{6}$, by substituting Eq. 30 in Eq. 27, the stress-strain relation will be[46]:

$$\sigma_{xx} = E\left(\varepsilon_{xx} + \frac{\eta_\alpha^2}{16}\frac{\partial^2 \varepsilon_{xx}}{\partial x^2} + \frac{\eta_\alpha^2}{48}\frac{\partial^2 \varepsilon_{xx}}{\partial z^2} + \frac{3\eta_\alpha^2}{32}\frac{\partial^2 \varepsilon_{xz}}{\partial x\, \partial z}\right) \quad (33)$$

$$\sigma_{xz} = E\left(\frac{3}{4}\varepsilon_{xx} + \frac{3\eta_\alpha^2}{64}\frac{\partial^2 \varepsilon_{xz}}{\partial x^2} + \frac{\eta_\alpha^2}{64}\frac{\partial^2 \varepsilon_{xz}}{\partial z^2} + \frac{\eta_\alpha^2}{24}\frac{\partial^2 \varepsilon_{xx}}{\partial x\, \partial z}\right) \quad (34)$$

Since $\varepsilon_{xz} = \frac{\gamma_{xz}}{2}$ [46], so Eq. 31 and Eq. 32 become:

$$\sigma_{xx} = E\left(\varepsilon_{xx} + \frac{\eta_\alpha^2}{12}\frac{\partial^2 \varepsilon_{xx}}{\partial x^2} + \frac{\eta_\alpha^2}{64}\frac{\partial^2 \gamma_{xz}}{\partial x\, \partial z}\right) \quad (35)$$

$$\sigma_{xz} = E\left(\frac{3}{8}\gamma_{xz} + \frac{\eta_\alpha^2}{128}\frac{\partial^2 \gamma_{xz}}{\partial x^2} + \frac{3\eta_\alpha^2}{128}\frac{\partial^2 \gamma_{xz}}{\partial z^2}\right) \quad (36)$$

And Eq. 33 and Eq. 34 become:

$$\sigma_{xx} = E\left(\varepsilon_{xx} + \frac{\eta_\alpha^2}{16}\frac{\partial^2 \varepsilon_{xx}}{\partial x^2} + \frac{\eta_\alpha^2}{48}\frac{\partial^2 \varepsilon_{xx}}{\partial z^2} + \frac{3\eta_\alpha^2}{64}\frac{\partial^2 \gamma_{xz}}{\partial x\, \partial z}\right) \quad (37)$$

$$\sigma_{xz} = E\left(\frac{3}{8}\gamma_{xz} + \frac{3\eta_\alpha^2}{128}\frac{\partial^2 \gamma_{xz}}{\partial x^2} + \frac{\eta_\alpha^2}{128}\frac{\partial^2 \gamma_{xz}}{\partial z^2} + \frac{\eta_\alpha^2}{24}\frac{\partial^2 \varepsilon_{xx}}{\partial x\, \partial z}\right) \quad (38)$$

The shear and normal strains are calculated in the same way as in the previous part in Eq. 12 and Eq. 13. Furthermore, the kinetic energy is computed using the same equation in the previous part (Eq. 14).

By substituting Eq. 12 and Eq. 13 in Eq. 35 and Eq. 36 or Eq. 37 and Eq. 38 and introducing the result in Eq. 4, the strain energy is achieved.

When CBT or FSDBT is applied, substituting Eq. 12 and Eq. 13 into Eq. 37 and Eq. 38 cause the third term in Eq. 12 and the first term in Eq. 13 to become zero during differentiation of γ_xz and ε_xx with respect to x and z. In contrast, when higher-order shear deformation theories are employed, these terms retain non-zero values, which can significantly influence the calculations and enhance the accuracy of the results.

5. Free Vibration of a Beam by Rayleigh-Ritz Method:

In order to change ϕ from an angle to a length parameter, we define the parameter α as

$$\alpha = \phi L \quad (39)$$

Moreover, to achieve the eigenvalue problem, we assume the time response to be harmonic as

$$u = u_s cos(\omega t) \quad (40)$$

$$w = w_s cos(\omega t) \quad (41)$$

$$\alpha = \alpha_s cos(\omega t) \quad (42)$$

where u_s, w_s and α_s are

$$u_s(x) = \sum_{i=1}^{q_m} D\, u_i \zeta_i^u(x) \quad (43)$$

$$w_s(x) = \sum_{i=1}^{q_m} D\, w_i \zeta_i^w(x) \quad (44)$$

$$\alpha_s(x) = \sum_{i=1}^{q_m} D\, \phi_i \zeta_i^\phi(x) \quad (45)$$

$$D = \begin{bmatrix} Du \\ Dw \\ D\alpha \end{bmatrix} \quad (46)$$

$$\zeta(x) = \begin{bmatrix} \zeta^u(x) \\ \zeta^w(x) \\ \zeta^\alpha(x) \end{bmatrix} \quad (47)$$

here, q_m is the number of admissible functions taken into account. $\zeta^u(x)$, $\zeta^w(x)$ and $\zeta^\alpha(x)$ are the admissible functions for u, w, α respectively, that should be compatible with the system's geometric boundary conditions. The geometric boundary conditions for the three considered nanobeams in this work are shown in Table 2.

Table 2. Geometric boundary conditions for three different boundary conditions [18]

Boundary condition	$x = 0$	$x = L$
C-F	$u = 0, w = 0,$ $\phi = 0, \frac{dw}{dx} = 0$	$u \neq 0, w \neq 0,$ $\phi \neq 0, \frac{dw}{dx} \neq 0$
S-S	$u \neq 0, w = 0,$ $\phi \neq 0, \frac{dw}{dx} \neq 0$	$u \neq 0, w = 0,$ $\phi \neq 0, \frac{dw}{dx} \neq 0$
C-S	$u = 0, w = 0,$ $\phi = 0, \frac{dw}{dx} = 0$	$u \neq 0, w = 0,$ $\phi \neq 0, \frac{dw}{dx} \neq 0$

We use the following admissible functions for the three beams studied here.

For the simply supported-simply supported beam, we use:

$$\zeta_i^u(x) = cos\left(i\frac{x}{L}\pi\right) \tag{48}$$

$$\zeta_i^w(x) = sin\left(i\frac{x}{L}\pi\right) \tag{49}$$

$$\zeta_i^\alpha(x) = cos\left(i\frac{x}{L}\pi\right) \tag{50}$$

For the clamped-free beam, we use:

$$\zeta_i^u(x) = sin\left((2i-1)\frac{x}{L}\frac{\pi}{2}\right) \tag{51}$$

$$\zeta_i^w(x) = cos\left((2i-1)\frac{x}{L}\frac{\pi}{2}\right) - cosh\left((2i-1)\frac{x}{L}\frac{\pi}{2}\right) - C_i^{\zeta^w(x)}\left(sin\left((2i-1)\frac{x}{L}\frac{\pi}{2}\right) - sinh\left((2i-1)\frac{x}{L}\frac{\pi}{2}\right)\right) \tag{52}$$

$$\zeta_i^\alpha(x) = sin\left((2i-1)\frac{x}{L}\frac{\pi}{2}\right) \tag{53}$$

where

$$C_i^{\zeta^w(x)} = \frac{cos\left((2i-1)\frac{\pi}{2}\right)+cosh\left((2i-1)\frac{\pi}{2}\right)}{sin\left((2i-1)\frac{\pi}{2}\right)+sinh\left((2i-1)\frac{\pi}{2}\right)} \tag{54}$$

For the clamped-simply supported beam, we use:

$$\zeta_i^u(x) = sin\left((2i-1)\frac{x}{L}\frac{\pi}{2}\right) \tag{55}$$

$$\zeta_i^w(x) = cos\left((2i-1)\frac{x}{L}\frac{\pi}{2}\right) - cosh\left((2i-1)\frac{x}{L}\frac{\pi}{2}\right) - D_i^{\zeta^w(x)}\left(sin\left((2i-1)\frac{x}{L}\frac{\pi}{2}\right) - sinh\left((2i-1)\frac{x}{L}\frac{\pi}{2}\right)\right) \tag{56}$$

$$\zeta_i^\alpha(x) = sin\left((2i-1)\frac{x}{L}\frac{\pi}{2}\right) \tag{57}$$

where

$$D_i^{\zeta^w(x)} = \frac{cos\left((2i-1)\frac{\pi}{2}\right)-cosh\left((2i-1)\frac{\pi}{2}\right)}{sin\left((2i-1)\frac{\pi}{2}\right)-sinh\left((2i-1)\frac{\pi}{2}\right)} \tag{58}$$

According to the Reighley-Ritz method [48], the maximum strain energy and kinetic energy are calculated by substituting Eq. 39, Eq. 40, and Eq. 41 in the strain energy and kinetic energy equations and setting sin(ωt) or cos(ωt) equal to 1. Therefore:

$$T_{max} = \omega^2 \frac{1}{2}\int_0^L \int_{-0.5h}^{0.5h}\int_{-0.5b}^{0.5b}((\rho_c - \rho_m)\left(\frac{z}{h}+0.5\right)^k + \rho_m)\left(\frac{\partial u_x^{s\,2}}{\partial t} + \frac{\partial u_z^{s\,2}}{\partial t}\right)dv \tag{59}$$

$$u_x^s = u_s - z\frac{\partial w_s}{\partial x} + f_z\left(\frac{\partial w_s}{\partial x} - \varphi_s\right) \tag{60}$$

$$u_z^s = w_s \tag{61}$$

Finally, the eigenvalue problem will be [48]:

$$\frac{\partial U_{max}}{\partial D_p} - \omega^2 \frac{\partial T_{max}^2}{\partial D_p} = 0 \tag{62}$$

where p varies between 1 and $3q_m$ as q_m admissible functions are used for u, w and alpha, respectively so the total number of admissible functions will be $3q_m$.

6. Numerical Example

6.1. Parameters Value

The FG beam considered in this paper, is a combination of metal (Aluminum) and ceramic (Alumina), and the mechanical properties of this beam vary along its thickness (along the Z axis). The mechanical properties of Aluminum and Alumina are illustrated in Table 3. The variation of these properties along thickness for different values if power-law index is illustrated in illustrated in Figure 5, Fig. 6 and Fig. 7.

For a value of $k = 1$, The mechanical properties exhibit a linear variation. However, as the value of k increases, ceramic behavior

becomes more significant, while a lower value of k results in more prominent metal behavior. As it was mentioned in chapter 4, $\nu = \frac{1}{3}$. The beam has a square cross section where $b = h = 2nm$.

The dimensionless eigenfrequencies are calculated by Eq. 63 [46]:

$$\lambda_p = \frac{\omega L^2}{h}\sqrt{\frac{\rho_m}{E_m}} \tag{63}$$

Table 3. Mechanical properties of Aluminum and Alumina

Mechanical properties	Aluminum (metal)	Alumina (ceramic)
$\rho\ (kg/m^3)$	2702	3960
E (Gpa)	70	380

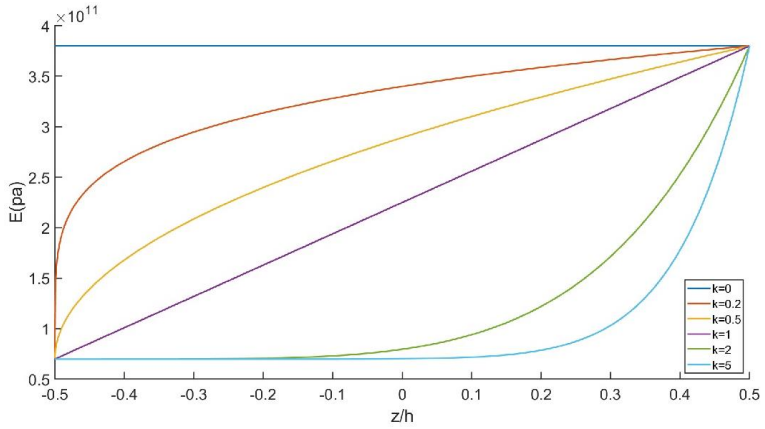

Fig. 5. Variation of modulus of elasticity along the beam thickness with different values of k

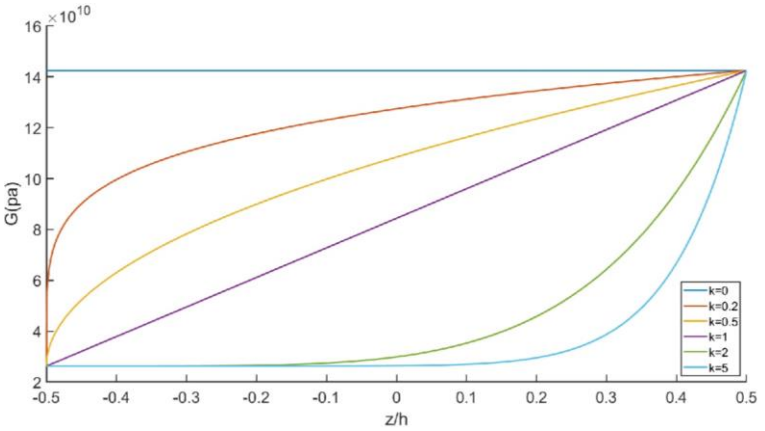

Fig. 6. Variation of shear modulus along the beam thickness with different values of k

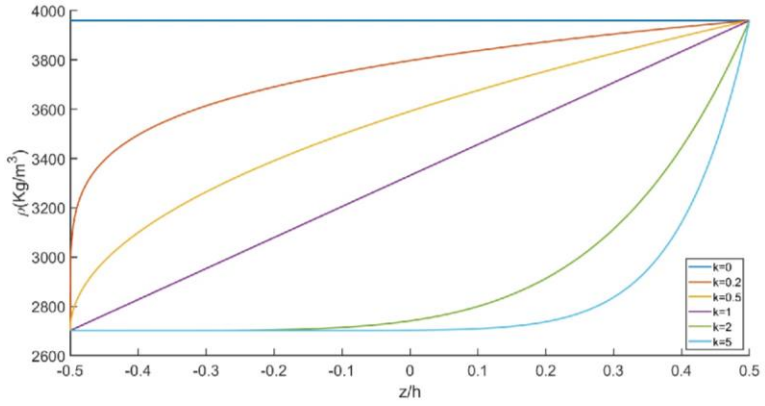

Fig. 7. Variation of density along beam thickness with different values of k

6.2. Verification of Natural Frequency of a Functionally Graded Beam with Different Shear Deformation Theories and Convergence of Results

The dimensionless eigenfrequencies the FG nanobeam with S-S, C-F and C-S boundary conditions for different shear deformation theories and for different number of admissible functions are shown in Table 4, Table 5 and Table 6, respectively.

In these tables, NAF is number of admissible functions being used. According to Table 4, Table 5 and Table 6, using 2 admissible functions for S-S, 4 admissible functions for C-F and 6 admissible functions for C-S result in appropiate accuracy. Based on the number of admissible functions, it can be inferred that utilizing admissible functions that are similar to shape functions can reduce the required number of admissible functions. As can be seen from these tables, all of the results are verified by other works [9, 18].

Table 4. Convergence and verification for natural frequencies of a FG $S-S$ beam

($E_m = 70Gpa$, $E_c = 380Gpa$, $\rho_m = 2702\frac{kg}{m^3}$, $\rho_c = 3960\frac{kg}{m^3}$, $k = 1$, $\nu = 0.3$, $\frac{L}{h} = 5$, $\lambda_p = \frac{\omega L^2}{h}\sqrt{\frac{\rho_m}{E_m}}$, NAF:Number of Admissible Functions)

NAF	1	2	3	Simsek [18]
CBT	4.14835	4.14835	4.14835	4.14835
FSDBT	3.99024	3.99024	3.99024	3.99023
PSDBT	3.99041	3.99041	3.99041	3.99042
TSDBT	3.99067	3.99067	3.99067	3.99067
HSDBT	3.99041	3.99041	3.99041	3.99042
ESDBT	3.99139	3.99139	3.99139	3.99139

Table 5. Convergence and verification for natural frequencies of a FG $\mathbf{C-F}$ beam

($E_m = 70Gpa$, $E_c = 380Gpa$, $\rho_m = 2702\frac{kg}{m^3}$, $\rho_c = 3960\frac{kg}{m^3}$, $k = 1$, $\nu = 0.3$, $\frac{L}{h} = 5$, $\lambda_p = \frac{\omega L^2}{h}\sqrt{\frac{\rho_m}{E_m}}$, NAF:Number of Admissible Functions)

NAF	1	2	3	4	5	6	Simsek [18]
CBT	12.68199	1.49324	1.49179	1.49162	1.49145	1.14143	1.49135
FSDBT	1.59367	1.47271	1.46585	1.46462	1.46423	1.46386	1.46300
PSDBT	1.40303	1.46941	1.46561	1.46439	1.46426	1.46390	1.46328
TSDBT	1.54305	1.46909	1.46564	1.46442	1.46432	1.46396	1.46339
HSDBT	12.66752	1.47226	146692	1.46633	1.46508	1.46496	1.46328
ESDBT	1.35085	1.46888	1.46574	1.46455	1.46446	1.46411	1.46357

Table 6. Convergence and verification for natural frequencies of a FG $\mathbf{C-S}$ beam

($E_m = 70Gpa$, $E_c = 380Gpa$, $\rho_m = 2702\frac{kg}{m^3}$, $\rho_c = 3960\frac{kg}{m^3}$, $k = 1$, $\nu = 0.3$, $\frac{L}{h} = 5$, $\lambda_p = \frac{\omega L^2}{h}\sqrt{\frac{\rho_m}{E_m}}$, NAF:Number of Admissible Functions)

NAF	2	3	4	5	6	Jin [9]
CBT $\frac{L}{h} = 20$	6.63536	6.59381	6.58970	6.58743	6.58670	6.58553
CBT	6.51163	6.46953	6.46570	6.46349	6.46282	-
FSDBT	6.04592	5.91227	5.88739	5.87678	5.87035	-
PSDBT	5.98361	5.90145	5.88386	5.87687	5.87215	-
TSDBT	5.97788	5.90141	5.88479	5.87825	5.87373	-
HSDBT	6.09965	5.95248	5.92560	5.90648	5.89657	-
ESDBT	5.97399	5.90304	5.88741	5.88130	5.87699	-

6.3. Verification of Natural Frequency of a Timoshenko Beam with Doublet Mechanics

To verify the results for DM method, natural frequencies of a S-S beam using FSDBT are compared with results of Gul [36]. It is noteworthy that instead of substituting ε_xz=γ_xz/2 in Eq. 33 and Eq. 34, Gul et al. [36] have multiplied the whole Eq. 34 by 1/2 so the coefficient of (∂^2 ε_xx)/∂x∂z in Eq. 34 is considered (η_α^2)/48 instead of (η_α^2)/24. Therefore, Gul et al. [36] have used Eq. 64 instead of Eq. 38. To confirm the results for the armchair structured beam, we compared the dimensionless natural frequencies of the beam using two different equations. The first equation used was Eq. 38, and the second equation used was Eq. 64, as referenced in Gul's paper [36].

The comparison results can be found in Table 8. It can be seen that using the correct coefficients in DM theory makes DM natural frequency prediction stiffened unlike Gul et al. [36] which predict softened natural frequencies. Regarding Table 7 and Table 8, it's important to note that Gul [36] calculated the natural frequencies for h=1. However, in some cases in both tables, η_α=2, which means that the beam width is considered less than atomic bond length (ηα). As a result, the value of h had to be adjusted to be more reasonable for the cases in Table 7 and Table 8. Thus, the results for h=2 are brought in Table 7 and Table 8 too. As it is seen in Table 7 and Table 8, with athe ssumptions ofthe [36], the results of this paper can be verified with results of Gul [36].

$$\sigma_{xz} = E\left(\frac{3}{8}\gamma_{xz} + \frac{3\eta_\alpha^2}{128}\frac{\partial^2\gamma_{xz}}{\partial x^2} + \frac{\eta_\alpha^2}{128}\frac{\partial^2\gamma_{xz}}{\partial z^2} + \frac{\eta_\alpha^2}{48}\frac{\partial^2\varepsilon_{xx}}{\partial x\,\partial z}\right) \tag{64}$$

Table 7. Verification of the doublet mechanics method for a **S** − **S** zigzag structured beam

(E = 30Mpa, ρ = $1\frac{\text{kg}}{\text{m}^3}$, λ = $\omega L^2\sqrt{\frac{\rho A}{EI}}$, κ = $\frac{5}{6}$, L = 10m, h = 2nm)

$\frac{L}{h}$	η_α	DM zigzag [36]	DM zigzag $h=1$	DM zigzag $h=2$
10	0	9.7074	9.7074	9.7044
	1	9.6682	9.6946	9.6651
	2	9.5493	9.6651	9.5464
20	0	9.8281	9.8273	9.8281
	1	9.8180	9.8248	9.8172
	2	9.7878	9.8172	9.7870
100	0	9.8679	9.8679	9.8679
	1	9.8675	9.8677	9.8674
	2	9.8663	9.8674	9.8662

Table 8. Verification of the doublet mechanics method for a **S** − **S** armchair structured beam

(E = 30Mpa, ρ = $1\frac{\text{kg}}{\text{m}^3}$, λ = $\omega L^2\sqrt{\frac{\rho A}{EI}}$, κ = $\frac{5}{6}$, L = 10m, h = 2nm)

$\frac{L}{h}$	η_α	Dm armchair [36]	Dm armchair Eq. 60, $h=1$	Dm armchair Eq. 38, $h=2$
10	0	9.7074	9.7074	9.7044
	1	9.7019	9.6989	9.7094
	2	9.6691	9.6665	9.7208
20	0	9.8281	9.8281	9.8273
	1	9.8268	9.8260	9.8276
	2	9.8188	9.8181	9.8317
100	0	9.8679	9.8679	9.8679
	1	9.8678	9.8678	9.8679
	2	9.8675	9.8675	9.8680

6.4. Effect of Power-Law Index on Natural Frequency of a Functionally Graded Beam using Doublet Mechanics for Various Shear Deformation Theories

Table 9, Table 10 and Table 11 demonstrate the impact of the power-law index on the natural frequency of both armchair and zigzag FG beams, as analyzed using DM theory. These tables are compared to the results obtained without utilizing DM theory. Based on the research conducted, it seems that CBT yields close natural frequencies for armchair and zigzag doublet mechanics, and close to those obtained through classical method. However, when using FSDBT or higher order shear deformation theories, the differences become significant.

Interestingly, the natural frequency of the armchair beam appears to be higher than that of the zigzag beam, and the natural frequency obtained with the classical method results generally fall somewhere in between. The effect of using doublet mechanics is approximately constant for different power-law indices. Table 9, Table 10, and Table 11, and Figure 5, Figure 6 and Figure 7 illustrate that an increase in the value of k leads to a more significant metallic behavior, resulting in a decrease in natural frequencies. Conversely, a lower value of k results in more prominent ceramic behavior, which can be observed through higher natural frequencies. In Table 9, Table 10, and Table 11, for k=0, mechanical properties are identical with pure ceramic.

Table 9. Effect of Power-Law Index on Natural Frequency of a $\boldsymbol{S-S}$ Functionally Graded Beam using Doublet Mechanics for Various Shear Deformation Theories

k	0	0.5	1	2	10	Pure Metal
CBT	5.39533	4.59313	4.14835	3.77930	3.49208	2.80336
CBT Zigzag	5.37309	4.57421	4.13125	3.76373	3.47769	2.79181
CBT Armchair	5.37866	4.57895	4.13553	3.76763	3.48129	2.79470
FSDBT	5.14665	4.40342	3.98641	3.63087	3.30919	2.67416
FSDBT Zigzag	5.12688	4.38637	3.97092	3.61677	3.29659	2.66388
FSDBT Armchair	5.15520	4.41085	3.99316	3.63696	3.31446	2.67860
PSDBT	5.14694	4.40625	3.98659	3.62275	3.27668	2.67430
PSDBT Zigzag	5.09574	4.36554	3.95040	3.58802	3.23545	2.64770
PSDBT Armchair	5.18294	4.43425	4.01125	3.64649	3.30612	2.69301
TSDBT	5.14734	4.40657	3.98686	3.62264	3.27615	2.67451
TSDBT Zigzag	5.09662	4.36601	3.95098	3.58891	3.23760	2.64816
TSDBT Armchair	5.18256	4.43408	4.01096	3.64570	3.30455	2.69281
HSDBT	5.14693	4.40625	3.98659	3.62278	3.27676	2.67430
HSDBT Zigzag	5.09563	4.36548	3.95032	3.58791	3.23520	2.64765
HSDBT Armchair	5.18299	4.43427	4.01128	3.64657	3.30628	2.69304
ESDBT	5.14845	4.40741	3.98759	3.62303	3.27643	2.67509
ESDBT Zigzag	5.09724	4.36630	3.95138	3.58958	3.23920	2.64848
ESDBT Armchair	5.18230	4.43401	4.01075	3.64498	3.30311	2.69268

Table 10. Effect of Power-Law Index on Natural Frequency of a $\mathbf{C-F}$ Functionally Graded Beam using Doublet Mechanics for Various Shear Deformation Theories

k	0	0.5	1	2	10	Pure Metal
CBT	1.93861	1.65060	1.49162	1.36018	1.25667	1.00728
CBT Zigzag	1.93908	1.65097	1.49191	1.36040	1.25693	1.00753
CBT Armchair	1.93904	1.65094	1.49189	1.36039	1.25691	1.00751
FSDBT	1.89610	1.61827	1.46394	1.33461	1.22489	0.98519
FSDBT Zigzag	1.89264	1.61532	1.46128	1.33219	1.22265	0.98340
FSDBT Armchair	1.89718	1.61923	1.46482	1.33541	1.22554	0.98576
PSDBT	1.89581	1.61848	1.46371	1.33292	1.21877	0.98504
PSDBT Zigzag	1.88816	1.61247	1.45840	1.32782	1.21242	0.98107
PSDBT Armchair	1.90275	1.62386	1.46847	1.33758	1.22464	0.98865
TSDBT	1.89587	1.61853	1.46375	1.33290	1.21870	0.98508
TSDBT Zigzag	1.88852	1.61271	1.45865	1.32813	1.21301	0.98126
TSDBT Armchair	1.90282	1.62394	1.46852	1.33754	1.22449	0.98869
HSDBT	1.89846	1.62059	1.46569	1.33500	1.22132	0.98642
HSDBT Zigzag	1.89510	1.61811	1.46343	1.33253	1.21755	0.98468
HSDBT Armchair	1.90809	1.62821	1.47237	1.34125	1.22867	0.99143
ESDBT	1.89607	1.61868	1.46388	1.33298	1.21879	0.98518
ESDBT Zigzag	1.88884	1.61292	1.45887	1.32840	1.21349	0.98142
ESDBT Armchair	1.90292	1.62403	1.46859	1.33752	1.22436	0.98874

Table 11. Effect of Power-Law Index on Natural Frequency of a $\boldsymbol{C-S}$ Functionally Graded Beam using Doublet Mechanics for Various Shear Deformation Theories

k	0	0.5	1	2	10	Pure Metal
CBT	8.40618	7.15643	6.46282	5.88660	5/43834	4/36778
CBT Zigzag	8.36030	7.11711	6.42693	5.85355	5/40824	4/34394
CBT Armchair	8.37285	7.12786	6.43673	5.86256	5/41647	4/35046
FSDBT	7.49062	6.45076	5.85715	5.33128	4/77297	3/89206
FSDBT Zigzag	7.41763	6.38735	5.79936	5.27873	4/72705	3/85414
FSDBT Armchair	7.49501	6.45734	5.86423	5.33742	4/77278	3/89435
PSDBT	7.49359	6.46168	5.85912	5.30545	4/67336	3/89361
PSDBT Zigzag	7.33820	6.33517	5.74642	5.19920	4/55732	3/81287
PSDBT Armchair	7.60848	6.55345	5.94114	5.38419	4/76179	3/95331
TSDBT	7.49598	6.46351	5.86076	5.30595	4/67309	3/89485
TSDBT Zigzag	7.35102	6.33957	5.75096	5.20476	4/56691	3/81623
TSDBT Armchair	7.60936	6.55461	5.94171	5.38300	4/75859	3/95376
HSDBT	7.52711	6.48864	5.88398	5.33046	4/70189	3/91103
HSDBT Zigzag	7.41491	6.39863	5.80255	5.25040	4/60867	3/85273
HSDBT Armchair	7.67254	6.60586	5.98755	5.42703	4/80678	3/98659
ESDBT	7.50090	6.46724	5.86411	5.30825	4/67548	3/89741
ESDBT Zigzag	7.35040	6.34348	5.75500	5.20965	4/57482	3/81921
ESDBT Armchair	7.61056	6.55601	5.94249	5.38201	4/75574	3/95438

6.5. Effect of Length Scale Parameter on Natural Frequency of a Functionally Graded Beam Using Doublet Mechanics for Various Shear Deformation Theories

Table 12, Table 13 and Table 14 showcase the effect of the length scale parameter on the natural frequency of FG beams using DM for different shear deformation theories. As observed, when ηα=0 (which is comparable to not employing DM), the natural frequency of armchair and zigzag structured beams remains equal. However, as ηα increases, the difference between them becomes more prominent. It's clear that the distinction becomes increasingly apparent when employing higher-order shear deformation theories, as opposed to CBT and FSDBT. As shown in Figure 8, Figure 10 and Figure 12, the natural frequency in zigzag structures declines as η_α increases, and this reduction is more pronounced when higher-order shear deformation theories are employed. Based on the findings from Figure 9, Figure 11 and Figure 13, it appears that in an armchair structure, increasing η_α results in a decrease in natural frequency according to CBT.

According to Figure 4, armchair structure is stiffer than zigzag structure along z axis. So, when analyzing transversal vibration of beams, when the length scale parameter is low, atomic structure does not affect beams' behavior significantly. However, when this parameter increases, the behavior of the beam tends to zigzag or armchair, and the effect of atomic structure becomes more noticeable. It can be seen that when the behavior tends to armchair, the beam becomes stiffer and natural frequencies increase, while when it tends to zigzag, it's the opposite. Moreover, using higher order shear deformation theories bolds this tendency more transparently and increases the precision and reliability of calculations significantly, especially for higher values of the length scale parameter.

However, shear deformation theories suggest a contrasting trend, with a significant rise observed. Observations indicate that the results of various higher-order shear deformation theories for S-S beams are similar, with no significant differences. However, for C-F and C-S beams, the dimensionless natural frequency computed using the HSDBT is slightly higher compared to other higher-order shear deformation theories. It is evident that at higher values of the length-scale parameter, or in nano and micro dimensions where dimensions are close to the length-scale parameter, the use of DM can significantly affect the natural frequencies. These findings highlight the importance of considering various theories and approaches in analyzing structural behavior. As mentioned in Section 4, incorporating higher-order shear deformation theories can account for additional terms in DM and lead to more accurate predictions of a beam's natural frequency. Conversely, using CBT may result in lower accuracy when predicting natural frequencies.

Table 12. Effect of Length Scale Parameter on Natural Frequency of a **S** − **S** Functionally Graded Beam using Doublet Mechanics for Various Shear Deformation Theories

η_α	0	0.21322	0.5	1	2
CBT Zigzag	4.14835	4.14757	4.14408	4.13125	4.07954
CBT Armchair	4.14835	4.14776	4.14515	4.13553	4.09685
FSDBT Zigzag	3.98641	3.98570	3.98254	3.97092	3.92403
FSDBT Armchair	3.98641	3.98674	3.98819	3.99316	4.00704
PSDBT Zigzag	3.98659	3.98508	3.97814	3.95040	3.74902
PSDBT Armchair	3.98659	3.98777	3.99299	4.01125	4.06479
TSDBT Zigzag	3.98686	3.98536	3.97846	3.95098	3.75471
TSDBT Armchair	3.98686	3.98801	3.99311	4.01096	4.06363
HSDBT Zigzag	3.98659	3.98508	3.97812	3.95032	3.74785
HSDBT Armchair	3.98659	3.98777	3.99300	4.01128	4.06489
ESDBT Zigzag	3.98759	3.98608	3.97913	3.95138	3.75084
ESDBT Armchair	3.98759	3.98869	3.99359	4.01075	4.06199

Table 13. Effect of Length Scale Parameter on Natural Frequency of a **C** − **F** Functionally Graded Beam using Doublet Mechanics for Various Shear Deformation Theories

η_α	0	0.21322	0.5	1	2
CBT Zigzag	1.49162	1.49164	1.49175	1.49191	1.48806
CBT Armchair	1.49162	1.49164	1.49172	1.49189	1.49031
FSDBT Zigzag	1.46394	1.46382	1.46328	1.46128	1.45279
FSDBT Armchair	1.46394	1.46398	1.46418	1.46482	1.46640
PSDBT Zigzag	1.46371	1.46349	1.46249	1.45840	1.42486
PSDBT Armchair	1.46371	1.46394	1.46495	1.46847	1.47981
TSDBT Zigzag	1.46375	1.46354	1.46258	1.45865	1.42667
TSDBT Armchair	1.46375	1.46398	1.46499	1.46852	1.47993
HSDBT Zigzag	1.46569	1.46564	1.46533	1.46343	1.43141
HSDBT Armchair	1.46569	1.46602	1.46747	1.47237	1.48529
ESDBT Zigzag	1.46388	1.46367	1.46273	1.45887	1.42665
ESDBT Armchair	1.46388	1.46410	1.46510	1.46859	1.47994

Table 14. Effect of Length Scale Parameter on Natural Frequency of a C − S Functionally Graded Beam using Doublet Mechanics for Various Shear Deformation Theories

η_α	0	0.21322	0.5	1	2
CBT Zigzag	6.46282	6/46136	6/45462	6/42694	6.12977
CBT Armchair	6.46282	6/46173	6/45671	6/43674	6/30846
FSDBT Zigzag	5.85715	5/85459	5/84298	5/79937	5/36305
FSDBT Armchair	5.85715	5/85764	5/85964	5/86423	5.84621
PSDBT Zigzag	5.85912	5/85441	5/83278	5/74642	5.09922
PSDBT Armchair	5.85912	5/86304	5/88045	5/94115	6.16906
TSDBT Zigzag	5.86076	5/85617	5/83508	5/75096	5.13560
TSDBT Armchair	5.86076	5/86463	5/8818	5/94171	6.16926
HSDBT Zigzag	5.88398	5/88104	5/86693	5/80256	4.95720
HSDBT Armchair	5.88398	5/88905	5/91141	5/98756	6.20760
ESDBT Zigzag	5.86411	5/85956	5/83864	5/75501	5.13835
ESDBT Armchair	5.86411	5/86785	5/88447	5/94249	6.16703

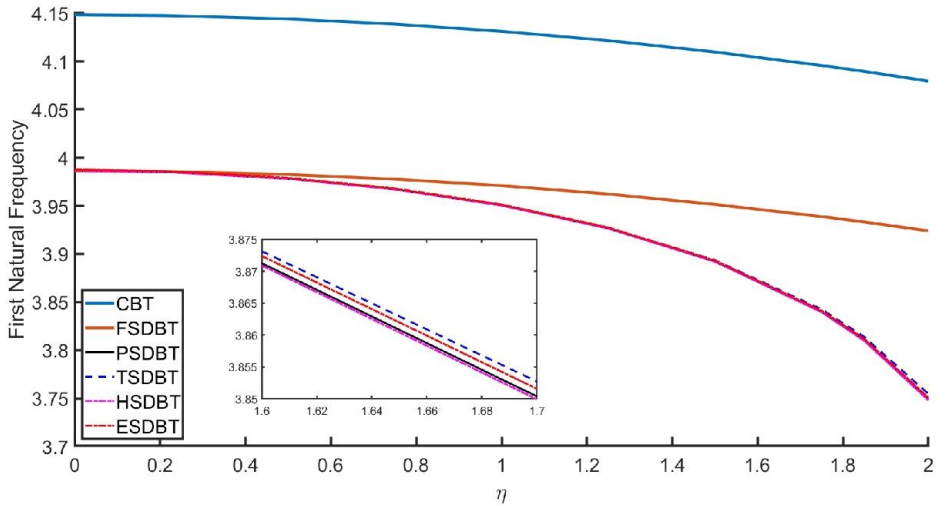

Fig. 8. Effect of length scale parameter η_α on a S − S zigzag-structured beam

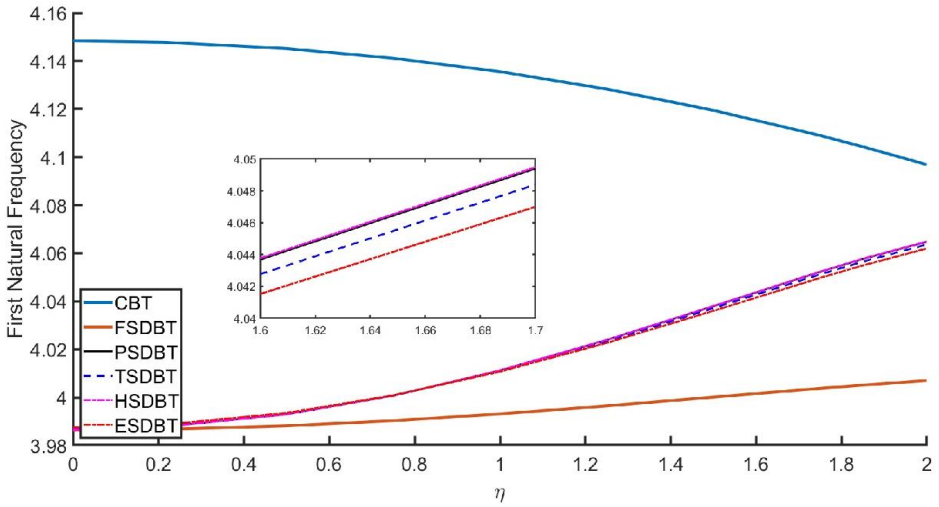

Fig. 9. Effect of length scale parameter η_α on a $S - S$ armchair structured beam

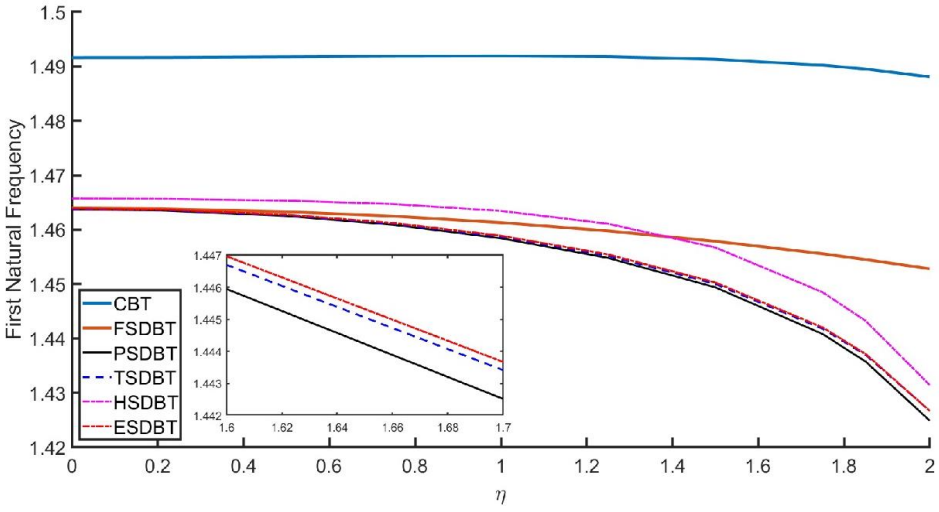

Fig. 10. Effect of length scale parameter η_α on a C − F zigzag structured beam

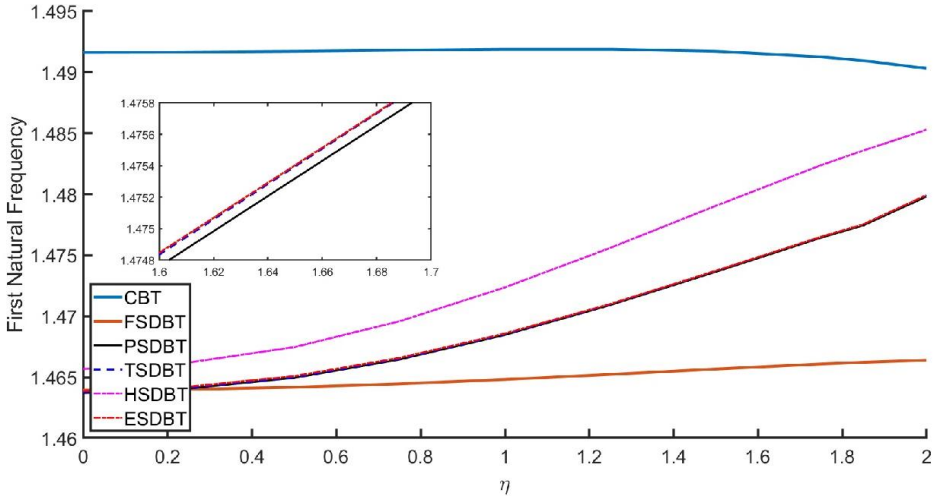

Fig. 11. Effect of length scale parameter η_α on a C − F armchair structured beam

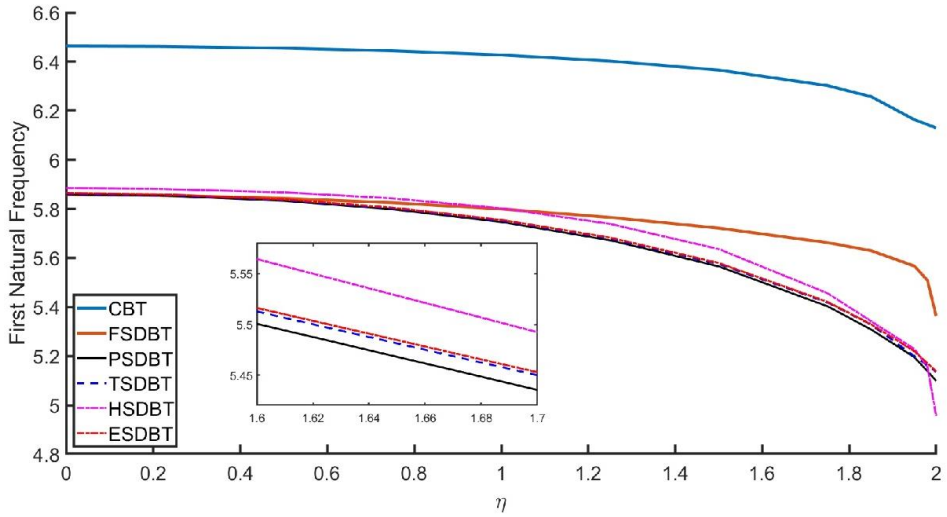

Fig. 12. Effect of length scale parameter η_α on a C − S zigzag structured beam

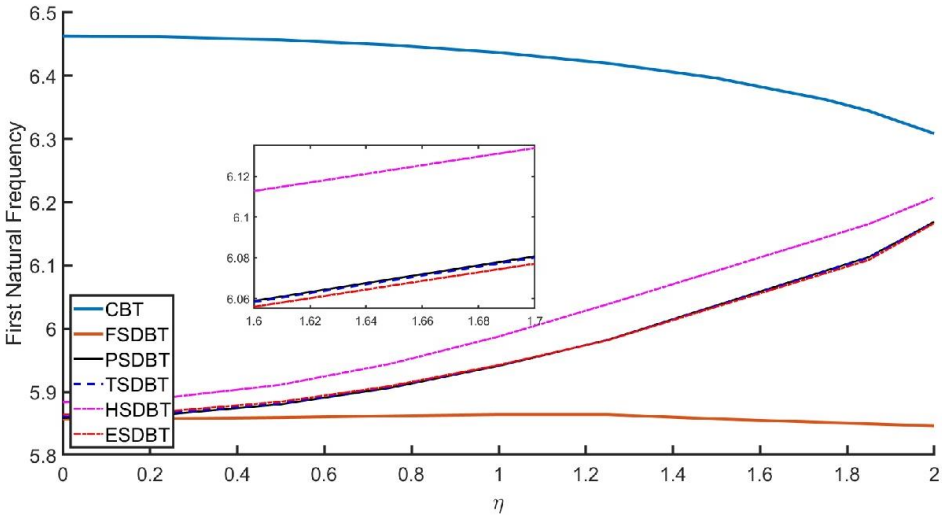

Fig. 13. Effect of length scale parameter η_α on a C − S armchair structured beam

6.6. *Effect of $\frac{L}{h}$ on Natural Frequency of a Functionally Graded Beam Using Doublet Mechanics for Various Shear Deformation Theories*

Table 15, Table 16, and Table 17 demonstrate the impact of the aspect ratio $\frac{L}{h}$ on the natural frequencies of FG beams using doublet mechanics with different shear deformation theories. The results indicate that increasing $\frac{L}{h}$ leads to an increase in ddimensionlessnatural frequencies for armchair, zigzag, and ordinary beams. Notably, the frequency differences between these three types of beams diminish as $\frac{L}{h}$ increases. The differences between the natural frequencies of the three types of beams are particularly noticeable at smaller values of $\frac{L}{h}$, especially when higher order shear deformation theories are employed. As shown in Fig. 14, Fig. 16 and Fig. 18, an abrupt increase in natural frequency occurs for all shear deformation theories as $\frac{L}{h}$ increases up to a value of 15. After this threshold, the rate of increase in dimentionless natural frequency slows down. In Fig. 15, Fig. 17 and Fig. 19, we have plotted the difference of natural frequencies for $S-S$, $C-S$, and $C-F$ beams so we can see a comparison between the natural frequencies obtained from DM and the classical method, for different beam theories. Interestingly, we observe that the zigzag and armchair DM methods produce close results for CBT. However, for $S-S$ and $C-S$ beams, dimensionless natural frequencies obtained using DM are lower than those obtained using the classical method for both armchair and zigzag structured beams. However, for $C-F$ beams, the dimensionless natural frequencies obtained using DM are higher than those obtained using the classical method.

For shear deformation theories, the dimensionless natural frequencies of DM armchair structures are higher than those obtained with classical theory, whereas the dimensionless natural frequencies of DM zigzag structures are lower than those obtained with classical theory which is due to armchair structure being stiffer. Both differences vanish by increasing $\frac{L}{h}$. To conclude, DM natural frequency predictions converge to natural frequencies obtained from classical methods when $\frac{L}{h}$ value exceeds 50. It is worth noting that the impact of using DM theory is more pronounced when $\frac{L}{h}<15$ and when using higher order shear deformation theories because when the thickness is constant, by increasing $\frac{L}{h}$ the length increases, and the effect of nanostructure decreases, and the difference of zigzag and armchair structures behavior vanishes.

Overall, these findings highlight the importance of considering different beam theories and methods to accurately predict natural frequencies.

Table 15. Effect of $\frac{L}{h}$ on Natural Frequency of a $S-S$ Functionally Graded Beam using Doublet Mechanics for Various Shear Deformation Theories

η_α	5	10	20	100
CBT	4.14835	4.20249	4.21634	4.22080
CBT Zigzag	4.13125	4.19817	4.21525	4.22075
CBT Armchair	4.13553	4.19925	4.21553	4.22076
FSDBT	3.98641	4.15748	4.20476	4.22033
FSDBT Zigzag	3.97092	4.15327	4.20368	4.22028
FSDBT Armchair	3.99316	4.15964	4.20534	4.22035
PSDBT	3.98659	4.15749	4.20476	4.22033
PSDBT Zigzag	3.95040	4.14716	4.20208	4.22022
PSDBT Armchair	4.01125	4.16466	4.20663	4.22040
FSDBT	3.98686	4.15756	4.20478	4.22033
TSDBT Zigzag	3.95098	4.14732	4.20212	4.22022
TSDBT Armchair	4.01096	4.16459	4.20661	4.22040
HSDBT	3.98659	4.15749	4.20476	4.22033
HSDBT Zigzag	3.95032	4.14714	4.20208	4.22022
HSDBT Armchair	4.01128	4.16467	4.20663	4.22040
ESDBT	3.98759	4.15776	4.20483	4.22033
ESDBT Zigzag	3.95138	4.14743	4.20215	4.22022
ESDBT Armchair	4.01075	4.16453	4.20660	4.22040

Table 16. Effect of $\frac{L}{h}$ on Natural Frequency of a $\boldsymbol{C-F}$ Functionally Graded Beam using Doublet Mechanics for Various Shear Deformation Theories

η_α	5	10	20	100
CBT	1.49162	1.50087	1.50321	1.50396
CBT Zigzag	1.49191	1.50101	1.50325	1.50396
CBT Armchair	1.49189	1.50098	1.50324	1.50396
FSDBT	1.46394	1.49437	1.50342	1.50963
FSDBT Zigzag	1.46128	1.49372	1.50325	1.50963
FSDBT Armchair	1.46482	1.49465	1.50349	1.50964
PSDBT	1.46371	1.49392	1.50293	1.50905
PSDBT Zigzag	1.45840	1.49231	1.50236	1.50881
PSDBT Armchair	1.46847	1.49511	1.50316	1.50899
FSDBT	1.46375	1.49388	1.50286	1.50897
TSDBT Zigzag	1.45865	1.49232	1.50231	1.50873
TSDBT Armchair	1.46852	1.49507	1.50310	1.50891
HSDBT	1.46569	1.49417	1.50170	1.50499
HSDBT Zigzag	1.46343	1.49347	1.50150	1.50487
HSDBT Armchair	1.47237	1.49591	1.50211	1.50495
ESDBT	1.46388	1.49386	1.50280	1.50888
ESDBT Zigzag	1.45887	1.49232	1.50225	1.50864
ESDBT Armchair	1.46859	1.49504	1.50303	1.50882

Table 17. Effect of $\frac{\mathbf{L}}{\mathbf{h}}$ on Natural Frequency of a $\mathbf{C-S}$ Functionally Graded Beam using Doublet Mechanics for Various Shear Deformation Theories

η_α	5	10	20	100
CBT	6/46282	6/56148	6/58671	6/59483
CBT Zigzag	6/42694	6/55324	6/58469	6/59475
CBT Armchair	6/43674	6/55534	6/5852	6/59477
FSDBT	5/85716	6/38356	6/54854	6/64077
FSDBT Zigzag	5/79937	6/36714	6/54429	6/64059
FSDBT Armchair	5/86423	6/3905	6/55049	6/64083
PSDBT	5/85913	6/38155	6/54467	6/63371
PSDBT Zigzag	5/74642	6/34347	6/53328	6/63083
PSDBT Armchair	5/94115	6/40966	6/55184	6/63323
FSDBT	5/86076	6/38165	6/54428	6/63277
TSDBT Zigzag	5/75096	6/3443	6/53311	6/62997
TSDBT Armchair	5/94171	6/40946	6/5514	6/6323
HSDBT	5/88399	6/39015	6/54294	6/59801
HSDBT Zigzag	5/80256	6/36189	6/53494	6/59716
HSDBT Armchair	5/98756	6/42382	6/5518	6/59805
ESDBT	5/86411	6/38231	6/54404	6/63184
ESDBT Zigzag	5/75501	6/34496	6/53289	6/62905
ESDBT Armchair	5/94249	6/40938	6/55099	6/63137

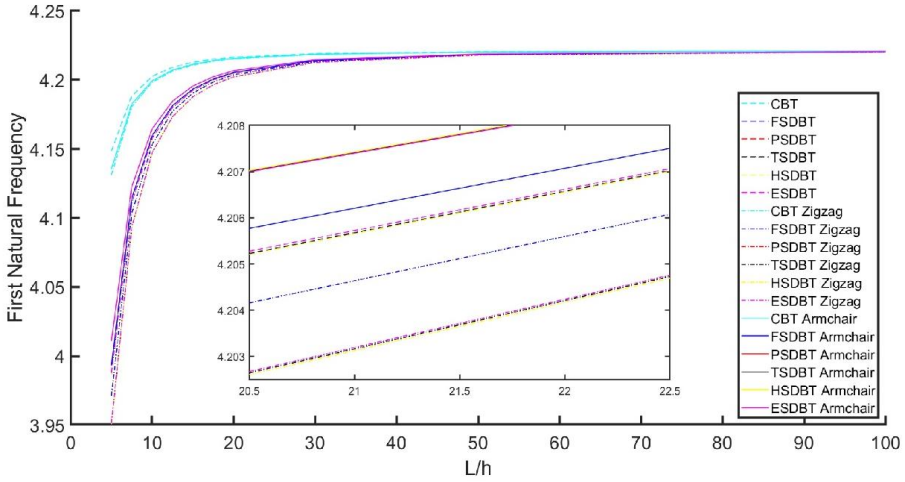

Fig. 14. Effect of $\frac{L}{h}$ on natural frequency of a S-S beam

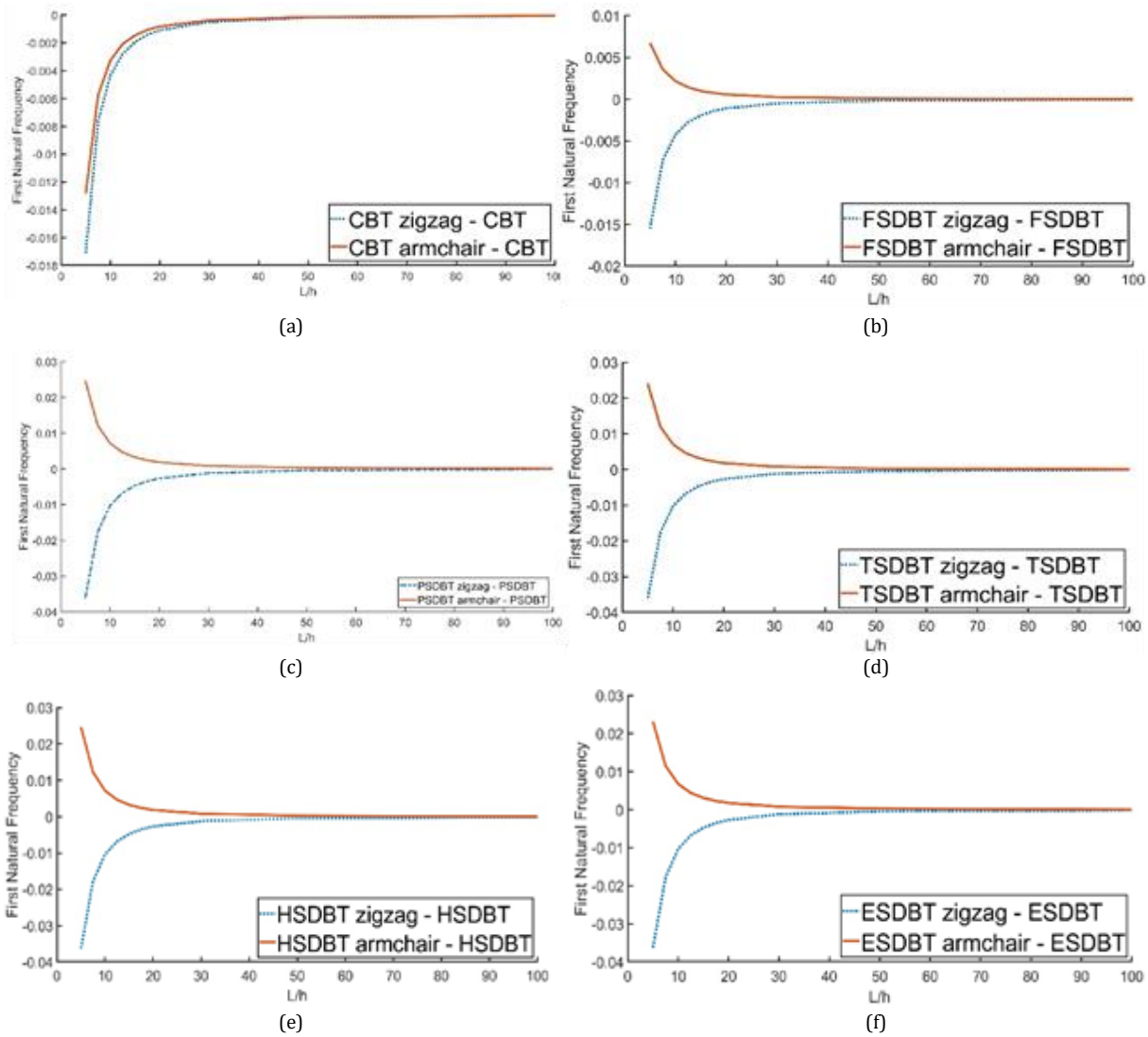

Fig. 15. Difference of natural frequencies obtained from DM and natural frequencies obtained from classical method for different beam theories for a S −S beam (a) CBT, (b) FSDBT, (c) PSDBT, (d) TSDBT, (e) HSDBT, (f) ESDBT

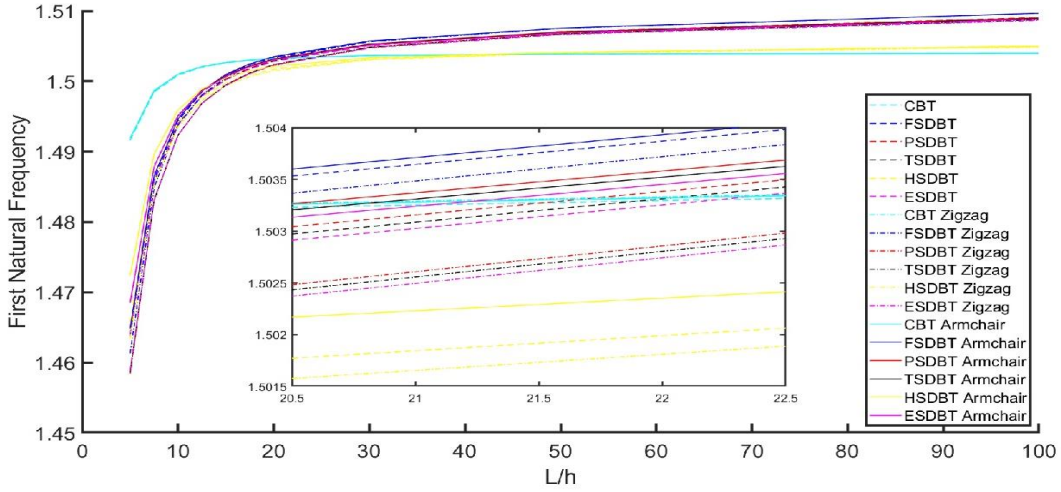

Fig. 16. Effect of $\frac{L}{h}$ on the natural frequency of a C-F beam

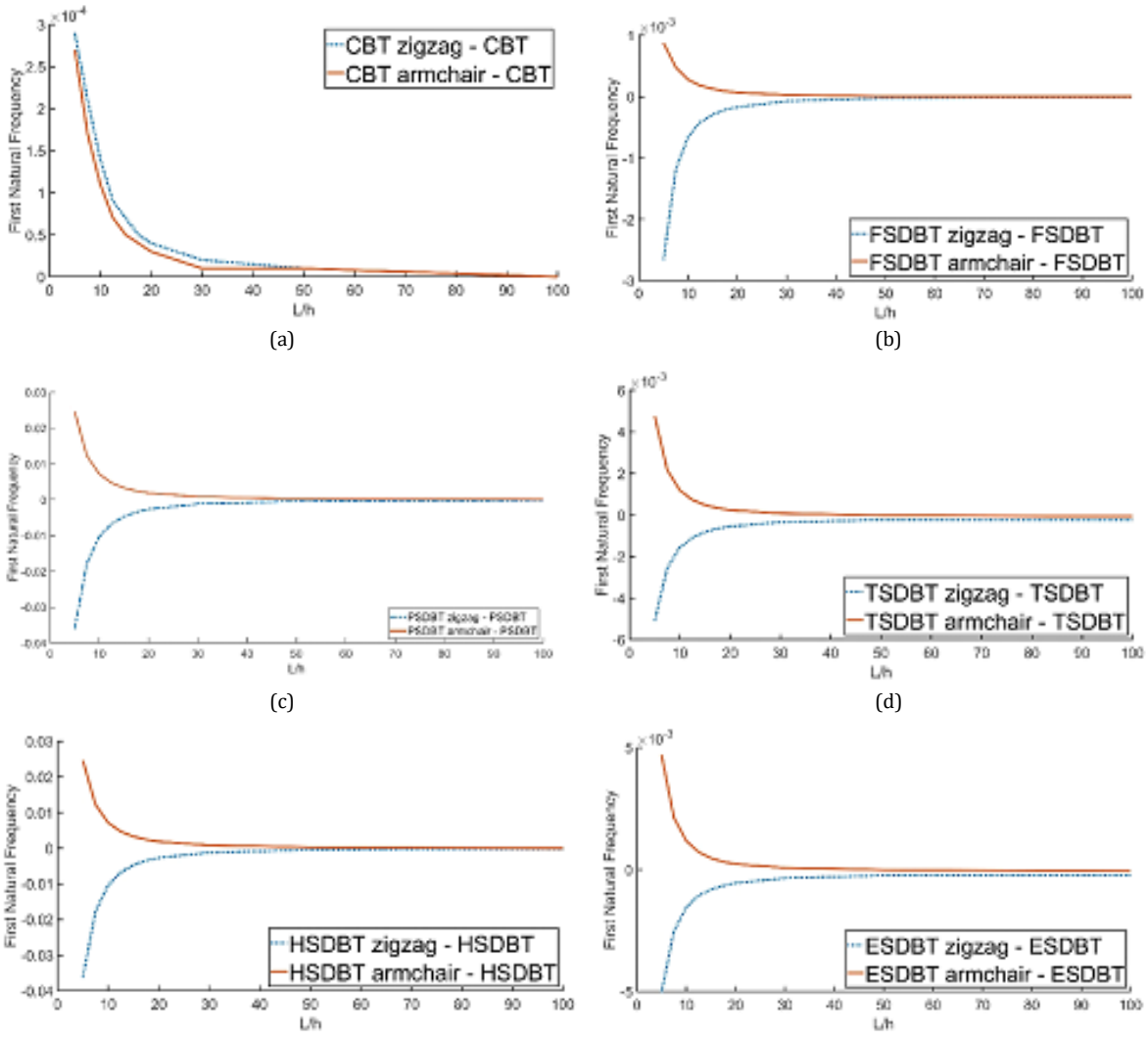

Fig. 17. Difference of natural frequencies obtained from DM natural frequencies obtained from classical method for different beam theories for a C −F beam (a) CBT, (b) FSDBT, (c) PSDBT, (d) TSDBT, (e) HSDBT, (f) ESDBT

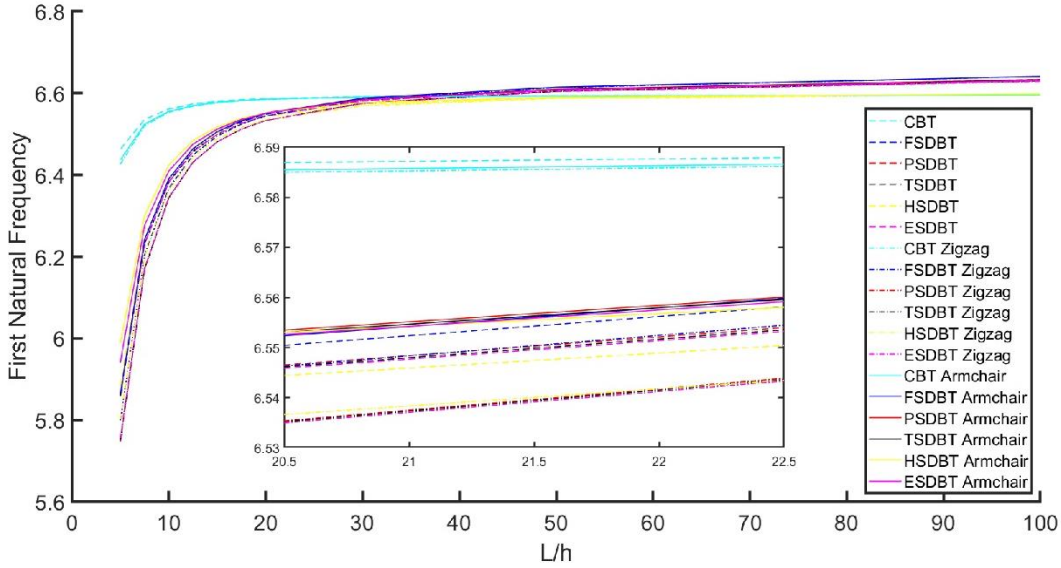

Fig. 18. Effect of $\frac{L}{h}$ on the natural frequency of a C-S beam

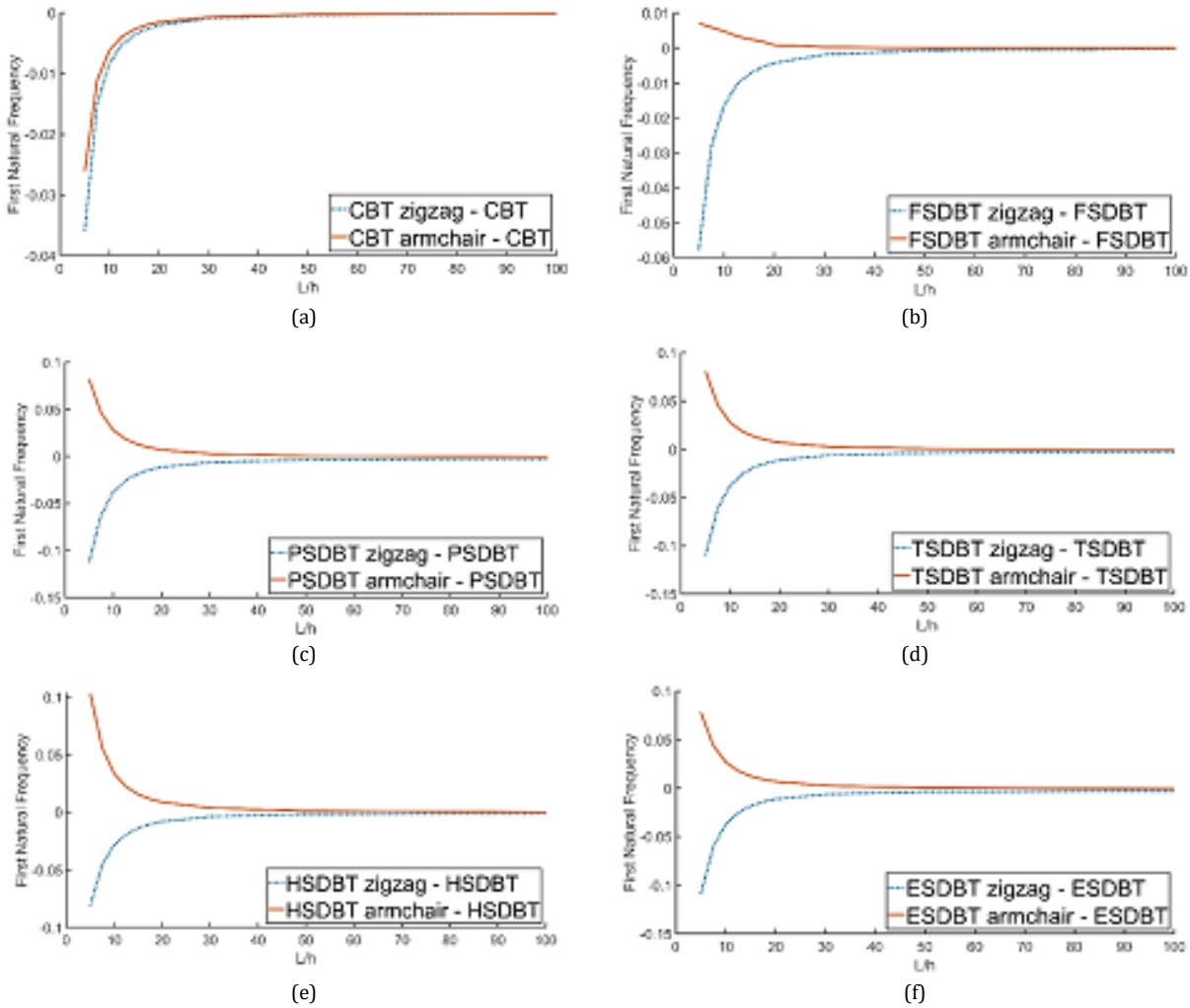

Fig. 19. Difference of natural frequencies obtained from DM and natural frequencies obtained from classical method for different beam theories for a C –S beam (a) CBT, (b) FSDBT, (c) PSDBT, (d) TSDBT, (e) HSDBT, (f) ESDBT

7. Conclusions

In this paper, we have investigated the vibration analysis of an FG nanobeam using DM theory with various shear deformation theories.

Due to the complexity of nanoscale structures, using doublet mechanics theory is advantageous as it describes the mechanical behavior of a structure using interactions of atoms. The DM theory can take into account the effect of atomic structure and the angle of atomic structure with respect to the beam direction. Although Euler-

Bernoulli beam theory (CBT) and Timoshenko beam theory (FSDBT) are commonly used in calculations; some terms in DM relations are omitted when applying these theories. To investigate the DM prediction more accurately, we utilized different higher-order shear deformation theories and compared the results with previous works. We applied our developed method to three nanobeams with three boundary conditions. We showed that considering the effect of higher-order shear deformation theories in DM theory has a notable effect on the free vibration analysis of these structures and can affect natural frequencies up to 5%.

Furthermore, we applied our proposed procedure to two different angles of atomic structure with respect to the longitudinal direction, which are called zigzag and armchair structured beams.

The results of our study indicate that the natural frequencies of zigzag-structured beams are lower than those predicted by ordinary theory, while the natural frequencies of armchair-structured beams are higher.

Furthermore, the effect of using DM theory is more pronounced when higher-order shear deformation theories are employed. This is because more terms of DM are taken into consideration in these theories, resulting in more accurate predictions of natural frequencies. Additionally, adjusting the atomic bond length ($\eta\alpha$) in DM can significantly impact the natural frequency of zigzag and armchair structured beams. Increasing $\eta\alpha$ causes a decrease in natural frequency for zigzag beams and an increase for armchair beams.

This accentuates the difference between the two structures. Our findings indicate that DM theory yields more pronounced effects for a lower ratio of length-to-thickness ($\frac{L}{h}$) values and it can result in more precision for nano and micro beams, especially for beams where $\frac{L}{h} < 10$.

Future studies can aim at forced response analysis of nanostructures using DM theory.

Funding Statement

This research did not receive any specific grant from funding agencies in the public, commercial, or not-for-profit sectors.

Conflicts of Interest

The author declares that there is no conflict of interest regarding the publication of this article.

References

[1] Filser, F. T., 2001. *Direct ceramic machining of ceramic dental restorations*. ETH Zurich.

[2] Knoppers, G., Gunnink, J., Van Den Hout, J. & Van Vliet, W., 2005. The reality of functionally graded material products. *Intelligent Production Machines and Systems: First I* PROMS Virtual Conference*, Elsevier, Amsterdam, pp. 467-474.

[3] Mahamood, R. M. & Akinlabi, E. T. 2017. Functionally graded materials, Springer.

[4] Azimi, M., Mirjavadi, S. S., Shafiei, N., Hamouda, A. & Davari, E., 2018. Vibration of rotating functionally graded Timoshenko nano-beams with nonlinear thermal distribution. Mechanics of Advanced Materials & Structures, 25, pp. 467-480.

[5] Zhong, Z., Chen, S., & Shang, E., 2010. Analytical solution of a functionally graded plate in cylindrical bending. *Mechanics of Advanced Materials Structures*, 17, pp. 595-602.

[6] Pradhan, K. & Chakraverty, S., 2013. Free vibration of Euler and Timoshenko functionally graded beams by Rayleigh–Ritz method. *Composites Part B: Engineering*, 51, pp. 175-184.

[7] Akgöz, B. & Civalek, Ö., 2013. Free vibration analysis of axially functionally graded tapered Bernoulli–Euler microbeams based on the modified couple stress theory. *Composite Structures, An International Journal*, 98, pp. 314-322.

[8] Akgöz, B. & Civalek, Ö., 2013. Buckling analysis of functionally graded microbeams based on the strain gradient theory. *Acta Mechanica*, 224, pp. 2185-2201.

[9] Jin, C., & Wang, X., 2015. Accurate free vibration analysis of Euler functionally graded beams by the weak form quadrature element method. *Composite Structures, An International Journal*, 125, pp. 41-50.

[10] Ansari, R., Gholami, R. & Sahmani, S., 2011. Free vibration analysis of size-dependent functionally graded microbeams based on the strain gradient Timoshenko beam theory. *Composite Structures, An International Journal*, 94, pp. 221-228.

[11] Attia, M. A., 2017. On the mechanics of functionally graded nanobeams with the account of surface elasticity. *International Journal of Engineering Science*, 115, pp. 73-101.

[12] Dehrouyeh-Semnani, A. M., Mostafaei, H. & Nikkhah-Bahrami, M., 2016. Free flexural vibration of geometrically imperfect functionally graded microbeams. *International Journal of Engineering Science*, 105, pp. 56-79.

[13] Fang, J., Gu, J. & Wang, H., 2018. Size-dependent three-dimensional free vibration of rotating functionally graded microbeams based on a modified couple stress theory. *International Journal of Mechanical Sciences*, 136, pp. 188-199.

[14] Rahmani, A., Babaei, A. & Faroughi, S., 2020. Vibration characteristics of functionally graded micro-beam carrying an attached mass. *Mechanics of Advanced Composite Structures*, 7, pp. 49-58.

[15] Sina, S., Navazi, H. & Haddadpour, H., 2009. An analytical method for free vibration analysis of functionally graded beams. *Materials Design*, 30, pp. 741-747.

[16] Li, X.-F., 2008. A unified approach for analyzing static and dynamic behaviors of functionally graded Timoshenko and Euler–Bernoulli beams. *Journal of Sound and vibration*, 318, pp. 1210-1229.

[17] Thai, H.-T. & Vo, T. P., 2012. Bending and free vibration of functionally graded beams using various higher-order shear deformation beam theories. *International journal of mechanical sciences*, 62, pp. 57-66.

[18] Şimşek, M., 2010. Fundamental frequency analysis of functionally graded beams by using different higher-order beam theories. *Nuclear Engineering Design*, 240, pp. 697-705.

[19] Alimohammadi Madanouei, I. and Karamooz Mahdiabadi, M., 2025. Free and Forced Vibration Mitigation of Nonlinear Functionally Graded Beams Based on Higher-Order Shear Deformation Theories Using NES. *International Journal of Structural Stability and Dynamics*, *25*(23), 2550244.

[20] Ghobad, Y., Mahdiabadi, M. K. & Farrokhabadi, A., 2024. High-frequency vibration analysis of laminated composite plates using energy flow and shear deformation theories. *Thin-Walled Structures*, 205, 112524.

[21] Babaei, A., Noorani, M.-R. S. & Ghanbari, A., 2017. Temperature-dependent free vibration analysis of functionally graded micro-beams based on the modified couple stress theory. *Microsystem technologies*, 23, pp. 4599-4610.

[22] Van Vinh, P., 2025. A novel modified nonlocal strain gradient theory for comprehensive analysis of functionally graded nanoplates. *Acta Mechanica*, 236, pp. 173-204.

[23] Son, L. T., Vinh, P. V., Chinh, N. V. & M. Sedighi, H., 2025. High-frequency temperature-dependent vibration of nonlocal functionally graded sandwich nanoplates resting on elastic foundations. *Mechanics of Advanced Materials Structures*, 32, pp. 957-978.

[24] Son, L. T., Belarbi, M.-O., Tounsi, A., Ziou, H., Avcar, M. & Van Vinh, P., 2025. Nonlocal vibration analysis of functionally graded sandwich nanoplates resting on general viscoelastic foundations. *Mechanics of Advanced Materials Structures*, pp. 1-18.

[25] Van Vinh, P. & Tounsi, A., 2022. Free vibration analysis of functionally graded doubly curved nanoshells using nonlocal first-order shear deformation theory with variable nonlocal parameters. *Thin-Walled Structures*, 174, 109084.

[26] Alimoradzadeh, M., Sedighi, H. M., Van Vinh, P. & Sofiyev, A. H., 2025. Primary and secondary resonance characteristics of electro-thermo-mechanically loaded GNP-Reinforced MEMS beams: A microstructurally informed approach. *Mechanical Systems & Signal Processing*, 238, 113162.

[27] Uzun, B. & Yayli, M. Ö., 2024. Porosity and deformable boundary effects on the dynamic of nonlocal sigmoid and power-law FG nanobeams embedded in the Winkler–Pasternak medium. *Journal of Vibration*

Engineering & Technologies, 12, pp. 3193-3212.

[28] Ghazwani, M. H., Alnujaie, A., Tounsi, A. & Van Vinh, P., 2024. On the high-frequency analysis of exponentially graded nanobeams resting on Winkler–Pasternak foundations. *Journal of Vibration Engineering Technologies*, 12, pp. 8113-8130.

[29] Dadashi, M. and Mahdiabadi, M.K., 2025. Dynamic Analysis of Functionally Graded Sandwich Doubly Curved Nanoshells Using Variable Nonlocal Elasticity Theory. *International Journal of Structural Stability and Dynamics*, *25*(12), p.2550122.

[30] Ferrari, M., Granik, V. & Imam, A., 1997. Introduction to doublet mechanics. *Advances in Doublet Mechanics,* Springer, pp. 1-26.

[31] Gul, U. & Aydogdu, M., 2021. Dynamic analysis of functionally graded beams with periodic nanostructures. *Composite Structures, An International Journal*, 257, 113169.

[32] Granik, V., 1978. Microstructural mechanics of granular media, Technique Report IM/MGU 78-241, Institute of Mechanics of Moscow State University. Russian.

[33] Granik, V. T. & Ferrari, M., 1993. Microstructural mechanics of granular media. *Mechanics of Materials*, 15, pp. 301-322.

[34] Gul, U., Aydogdu, M. & Gaygusuzoglu, G., 2017. Axial dynamics of a nanorod embedded in an elastic medium using doublet mechanics. *Composite Structures, An International Journal*, 160, pp. 1268-1278.

[35] Gul, U. & Aydogdu, M., 2018. Noncoaxial vibration and buckling analysis of embedded double-walled carbon nanotubes by using doublet mechanics. *Composites Part B: Engineering*, 137, pp. 60-73.

[36] Gul, U. & Aydogdu, M., 2021. A micro/nano-scale Timoshenko-Ehrenfest beam model for bending, buckling and vibration analyses based on doublet mechanics theory. *European Journal of Mechanics-A/Solids*, 86, 104199.

[37] Abdelrahman, A. A., Shanab, R. A., Esen, I. & Eltaher, M. a. J. S., 2022. Effect of moving load on dynamics of nanoscale Timoshenko CNTs embedded in elastic media based on doublet mechanics theory. *Composite Structures, An International Journal*, 44, pp. 255-270.

[38] Eltaher, M., Abdelrahman, A. A. & Esen, I., 2021. Dynamic analysis of nanoscale Timoshenko CNTs based on doublet mechanics under moving load. *The European Physical Journal Plus*, 136, 705.

[39] Eltaher, M. A. & Mohamed, N., 2020. Nonlinear stability and vibration of imperfect CNTs by doublet mechanics. *Applied Mathematics & Computation*, 382, 125311.

[40] Eltaher, M. A., Mohamed, N. & Mohamed, S. A., 2020. Nonlinear buckling and free vibration of curved CNTs by doublet mechanics. *Smart Structures & Systems, An International Journal*, 26, pp. 213-226.

[41] Civalek, Ö., Uzun, B. & Yaylı, M. Ö., 2024. Longitudinal vibration analysis of FG nanorod restrained with axial springs using doublet mechanics. *Waves in Random Complex Media*, 34, pp. 4937-4959.

[42] Pradhan, K. K. & Chakraverty, S., 2014. Effects of different shear deformation theories on free vibration of functionally graded beams. *International Journal of Mechanical Sciences*, 82, pp. 149-160.

[43] Assie, A. E., Mohamed, S. M., Shanab, R. A., Abo-Bakr, R. M. & Eltaher, M. A. 2023. Static Buckling of 2D FG Porous Plates Resting on Elastic Foundation based on Unified Shear Theories. *Journal of Applied & Computational Mechanics,* 9, pp. 239-258.

[44] Shanab, R., Mohamed, S., Tharwan, M. Y., Assie, A. E. & Eltaher, M. A., 2022. Buckling of 2D FG Porous unified shear plates resting on elastic foundation based on neutral axis. *Steel & Composite Structures, An International Journal*, 45, pp. 729-747.

[45] Mohamed, S., Assie, A. E., Mohamed, N. & Eltaher, M. A., 2022. Static and stress analyses of bi-directional FG porous plate using unified higher order kinematics theories. *Steel & Composite Structures, An International Journal*, pp. 305-330.

[46] Karamanli, A., 2021. Structural behaviours of zigzag and armchair nanobeams using finite element doublet mechanics. *European Journal of Mechanics-A/Solids*, 89, 104287.

[47] Ferrari, M., Granik, V. T., Imam, A. & Nadeau, J. C., 2008. *Advances in doublet mechanics,* 45. Springer Science & Business Media.

[48] Rao, S. S., 2019. *Vibration of continuous systems*. John Wiley & Sons.